MSc Thesis, 30 ECTS
ISRN LUTVDG / (TVTG-5144) / 1-99 /(2015)

Extending the resolution of conventional deep seismic 3D surveys

An evaluation in extracting data from deep seismic acquisition surveys for near surface high resolution interpretations

Niklas Gustafsson
Teknisk geologi
Lunds Tekniska Högskola
Lunds Universitet

LUND
UNIVERSITY

Extending the resolution of conventional deep seismic 3D surveys

An evaluation in extracting data from deep seismic acquisition surveys for near surface high resolution interpretations

Niklas Gustafsson

Master's Thesis

Department of Engineering Geology
Faculty of Engineering
2015

Abstract

The main objective of this master's thesis is to evaluate a new processing method for extracting seismic conventional 3D streamer deep target data for shallow subsurface imaging. Deep target acquisitions have greater potential than it's conventional use. The aim of these acquisitions is to discover natural resources, in particular oil and gas, at several kilometres of depth. Before drilling it is most important to map possible geohazards, especially shallow ones. Also government requirements, risks for human lives and facility failure oblige actions to map geohazards.

A method on how to reprocess deep target data acquired in shallow water has been developed for improving imaging of the shallow subsurface. Shallow water in this case is about 75 meters, while shallow subsurface refer to down to approximately 750 meters. The new reprocessing sequence is based on performing interpolation, multiple reflection attenuation and statics correction with focus on the shallow subsurface. The main objective of the evaluation is to compare resulting image from the reprocessed 3D data with the initial image and an overlapping dedicated high resolution 2D acquisition image. The conclusion also includes a recommendation for if the high definition reprocessing sequence can aid a dedicated high resolution 2D survey, from the perspective of this case.

First a synthetic data model was made to investigate minimum detectable layers. Within the model a stratified earth model was set up and model parameters varied: dominant frequency of source wavelet, target layer thickness and velocity. The outcome became the foundation for investigating the frequency content reflected in the shallow layers. Frequency content is important for the question if thin layers could be resolved. This was the basis for the next step to analyse the imaging result from the investigated reprocessing sequence.

The new processing sequence contributes to a significant improvement to the resolution of the high definition shallow 3D processed image evaluated in this report, from close to the seabed and beyond the horizon of this report. The frequency content seems to be sufficient to be able to resolve layers for aiding interpretations of the shallow subsurface. One comparison between the imaging from the new processing sequence and imaging of dedicated high resolution 2D acquisition show that the 2D acquired data generates a better result from the seabed to about 200 to 300 milliseconds. Somewhere in that range of 200 to 300 milliseconds the imaging from the new processing sequence becomes the better alternative. Thus to reprocess deep target seismic 3D streamer data can, for this case, aid dedicated high resolution 2D acquisition both in setting up the survey as well as discover geohazards.

Acknowledgements

First of all I am grateful to my supervisor senior lecturer Roger Wisén at the department of Engineering Geology for the engagement and believing in my work. From the very first start Mr Wisén has been of great help. Furthermore I wish to express my gratitude to my supervisor Ph.D. Anna Droujinina at Maersk Oil for the enormous engagement and support throughout my learning process. Also for the highly interesting discussions, the wise comments and introducing me to the problem. Likewise I am thankful to my supervisor James Musser at Maersk Oil who made this master's thesis possible. Without Mr Musser this thesis would not have been viable. At last I want to thank Maersk Oil and everyone who have answered my questions, given me advice and somehow been part of this master's thesis at Maersk Oil and the department of Engineering Geology.

CONTENTS

CHAPTER 1

INTRODUCTION

1.1 Background

Geophysics refers to the study of the earth by the laws of physics. Exploring the earth's interior by geophysics involves measurement of physical properties. Each physical property is measured with a different technique. Methods used are named after the measures taken: gravity, electrical, magnetic, electromagnetic and seismic surveys. Depending on the investigated scale, both areal and vertical, and physical properties, different techniques are used. Geophysical investigation stretches from exploring the inner core of the earth to very shallow civil engineering investigations of the topmost layers. From data recovered, analysis derives probable subsurface distribution of the measured property. Empirically lots of properties have been tested for different types of rock. Geophysical analysis of the subsurface can never be absolutely sure in it is predictions. Drilling borehole gives a true understanding of the subsurface but at discrete locations. However drilling boreholes is very expensive.

In the exploration industry geophysics is a necessity to be able to cover large areas of investigation. Exploration comprises searching for natural resources. One single category of subsurface natural resources can be detected in several different geophysical surveys. Nevertheless seismic survey is the technique of most importance for the industry (Kearey et al., 2002) and most widely spread (ConocoPhillips, 2015). Seismic exploration surveys demand in general advanced equipment due to necessity of precisely interpreting an often deep and complex geology. At marine acquisitions special made vessels tow seismic

sources followed by long lines of highly advanced hydrophones in specific formations, and also ocean bottom receivers can be used. These surveys tend to be large scale operations over areas of hundreds of square kilometres with the main objectives to acquire data from 1000 to 4000 meters of depth. Exploration surveys provide massive amount of data, especially large scale 3D surveys. Since the 1990s 3D surveys have become the primary exploration tool due to better acquisition strategies and that computer capacity has increased while they have become cheaper (Bulat and Long, 2006). Conventional seismic surveys will in this report refer to the type of seismic acquisitions described above and in more detail in section 2.3 and 3.3.

Here the reader should be alerted that there is a glossary in appendix A. It can be helpful to a reader not familiar with this subject.

1.2 Field of research

In a secondary stage before drilling it is highly interesting to extract data from a prospecting survey for near surface interpretations. Therefore could a successful extraction of data be cost efficient and can potentially lead to improved geohazards identification and risk assessment. By near surface and shallow in this context means the seabed to depths about 500 meters.

When acquiring conventional narrow azimuth marine streamer seismic data, the acquisition parameters are customised to better image usually deep target (Bulat, 2005). To achieve high resolution imaging of the shallow subsurface, much shorter source to receiver offsets and denser receiver spacing are needed. Under certain conditions the deep seismic data can still be reprocessed to achieve high resolution required to image shallow targets and possible shallow geohazards. The source-receiver offset [1] in combination with receiver spacing and depth to the sea floor are highly important when considering the use of deep seismic acquisitions for near subsurface imaging (Selvage et al., 2012).

Due to the deep seismic streamer acquisition design, the nearest hydrophone offset records are usually missing on outer receiver cables and often on the inner streamers, as well. However, the missing traces can be interpolated or extrapolated using information from the neighbouring records. There are various processing techniques, which can produce satisfactory interpolation results using spatial, dip, hydrophone offset and direction information from the nearest traces [2]. The success of this procedure strongly depends on the size of holes to be filled and quality of the data. If signal to noise ratio is high, missing traces can be reconstructed with a high degree of confidence.

[1] See glossary in appendix A.
[2] See glossary in appendix A.

Survey geometry and source intensity are important circumstances for the outcome of the data acquisition. Therefore these circumstances will also affect the circumstances for interpretability of the subsurface.

1.3 Aim and objective

This report will focus on two questions. The first one is: can conventionally shallow water acquired narrow azimuth 3D data be improved for shallow subsurface imaging? Shallow water in this case is about 75 meters, while shallow subsurface refer to down to approximately 750 meters. The new and important circumstance is here that the conventional deep target 3D data is acquired in shallow water. The second question is regarded whether the answer of the first question is positive: how may high definition 3D imaging aid dedicated high resolution 2D site survey imaging? The answer to the second question will lead to a recommendation from the perspective of this specific case.

Hence the main objective will be to evaluate the resulting image of the new high definition 3D processing sequence. The evaluation will be conducted within three connecting areas of investigation. First a simple computerised model will be created to simulate data acquisition of a horizontal stratified earth. This simulation seeks the threshold values of three impacting resolution parameters: dominant frequency of the source wavelet, seismic wave propagation velocity and target layer thickness. Secondly an investigation of a constrained part, i.e. one single sail line, of the reprocessed data will be performed. The purpose of the investigation will be to examine the frequency content of the reprocessed data. Together with the result from the first simulated model an estimation of the resolution can be made. Thirdly and last the reprocessed high definition 3D data will be loaded in to an interpretation tool, together with the initial 3D data (before applying the reprocessing sequence) and an overlapping data from a dedicated high resolution 2D survey. These three data sets will be interpreted as volumes and compared as horizon picking and time slices. [3] The comparison seeks the answer to if the high definition reprocessing sequence will generate any improvements and how the reprocessed image relate to an image from a dedicated high resolution 2D survey.

The resulting reprocessed high definition 3D data was provided from Maersk Oil, together with the initial conventionally processed 3D data and processed dedicated high resolution 2D data. Maersk Oil provided no images, but only data. Neither was any processing for improving any data quality done within the constrictions of this master's thesis. Processing performed here will be in the context of investigating the frequency content of the already high definition processed 3D data.

[3] See glossary in appendix A.

CHAPTER 2

SEISMIC IMAGING

This master's thesis main focus is a change in a normal processing work flow. To be able to describe the work this chapter will describe the theory behind some of the most crucial parts of seismic surveys. Starting at the laws of physics which briefly describes seismic acquisition and ending at seismic processing.

2.1 Seismic waves

A seismic wave is an acoustic wave that propagates in the subsurface of the earth. This wave phenomenon is an oscillation of matter where only energy propagates. At a geological boundary some of the wave energy will split into refraction and reflection. The arrival time and amplitude of the returned wave is measured at different locations. The appearance of the oscillations requires an applied force. Often in seismic surveys these forces are fabricated from a source of energy release or heavy vibrating truck (Kearey et al., 2002). In a marine environment the most commonly used sources are several airguns in special formations called an airgun array. An airgun release is equivalent to the energy achieved by an explosive source, e.g. dynamite.

Stress and strain are the foundation of understanding seismic wave propagation. Apply an external force to a body and stresses will appear on the surface and spread internally. Stress is the force distributed over an area. Imagine a point in the body surrounded by an infinitesimal small cube with dimensions dx, dy and dz. Some stress acting upon one of the cube sides with arbitrary direction can

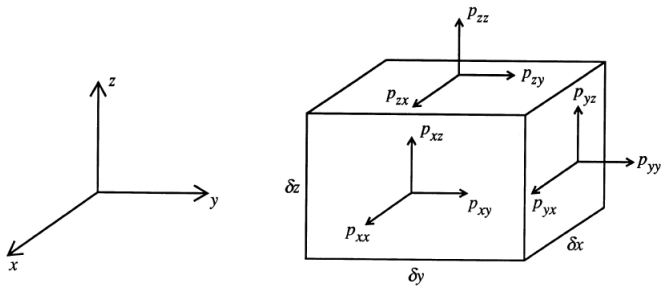

Figure 2.1: Stress components acting on an infinitesimally small volume, (Yilmaz, 2001)

be decomposed into three components, see figure 2.1. One component perpendicular to the plane called normal stress. The other two components will then be tangential to the plane and called shear stress. The normal stress causes a compressional wave, which is the fastest propagating wave, also called primary wave or P-wave. Likewise the shear stress causes a slower propagating wave called shear wave or S-wave. While this report focuses on an marine seismic data acquisition it is important to know that shear stress can not be supported by fluids, i.e. S-waves do not exist in fluids. In fluids only one stress component exist, the hydrostatic pressure, which propagates as a compressional wave, P-wave. Seismic waves normally propagate through the subsurface in a few thousands of kilometres per second. However oscillation of particles that carries the waves are small. Seismic waves acquired in surveys must be considered weak and cause ground displacements about 10^{-10} m and velocities about 10^{-8} m/s. Therefore strains are in the elastic field of the stress-strain curve for a normal survey except in the vicinity of the seismic source. While strains are biggest closely to the source this will not do any harm in a marine environment. The linear relationship between stress and strain are expressed as Young's modulus, E.

Seismic waves propagate differently why there are two groups of waves called surface waves and body waves. These two groups are easily subdivided depending on in how many dimensions the wave propagates. Surface waves only propagates along the surface of a body while body waves propagates three dimensionally through the internal volume, i.e. the subsurface. This study will only consider body waves. Both shear waves and compressional waves exist as body waves. Those types of waves are described in figure 2.2.

It is reasonable to assume denser material at greater depth in the subsurface in general. Denser materials provide the conditions for faster wave propagation. A steady increase of density is far from always the case. While this work focuses on finding shallow geological hazards it is important how the properties varies with the gas-bearing and water saturated rocks. S-waves cannot propagate in

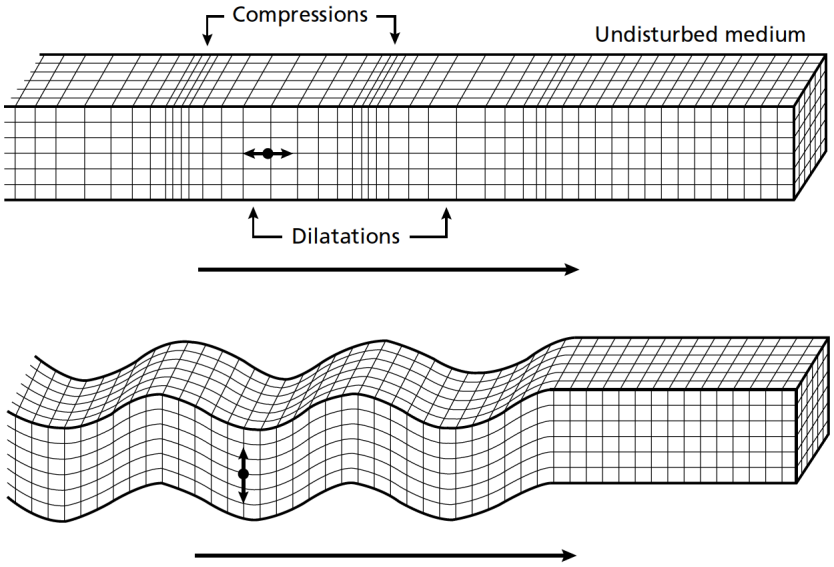

Figure 2.2: Describing compressional (top) and shear (bottom) wave propagation by oscillation in matter, (Kearey et al., 2002)

water and gas and always need to propagate within a solid. There seems to be a relationship between P-wave and S-wave velocity empirically determined for different rock types. Figure 2.3 shows how the velocities relates.

The P-wave and S-wave velocity cross-plot in figure 2.3 defines almost a straight line called the mudrock line. The line is defined by the equation

$$v_p = c_0 + c_1 v_s \tag{2.1}$$

where v_p, v_s are the P-wave and S-wave velocity and c_0, v_s are empirically determined for various types of rocks. For water saturated clastics [1] c_0 and c_1 are suggested to be 1360 and 1.16 (Yilmaz, 2001). As shown in figure 2.3 gas-bearing sandstones are creating a straight line with smaller gradient slightly over the water saturated clastics. Hence gas-bearing sandstone should generate a bigger scalar c_0 and smaller scalar c_1.

[1] See glossary in appendix A.

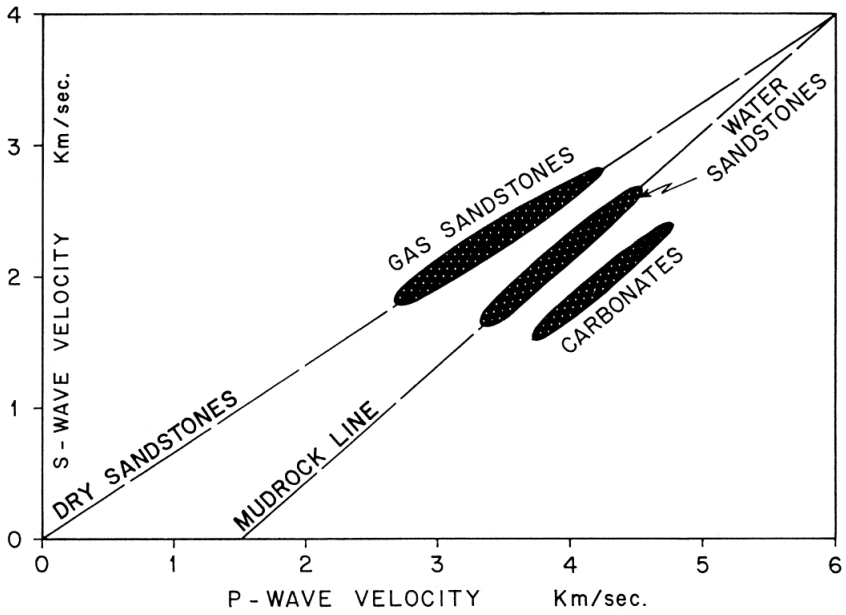

Figure 2.3: P-wave to S-wave velocity cross-plot, (Yilmaz, 2001). Modelling basis for layers S-wave velocity.

2.2 Raytracing

Seismic waves propagate spherically within materials without shifts in properties. When describing a ray it is referring to a one dimensional line from one point to another, such as from a source to a receiver. The line could be described in a two dimensional plane or a three dimensional volume, often depending on how the target survey is set up. The ray is also lined perpendicular to how the wave is expanding.

Intuitively, as for the real case, the amplitude decay along with the spherical wave propagates outwards from the source. One fixed amount of energy is set into motion with the wave. Whilst the propagation occurs the energy is speared over the area of the wavefront. Hence the amplitude, or energy per unit area, of the wavefront is inversely proportional to the square of the radius. The phenomenon is called spherical spreading.

Secondly energy attenuates along the path of propagation due to frictional dissipation of wave energy into heat. This frictional attenuation phenomenon is still subject to research. Different rock types show different frictional energy loss. Empirically one specific rock type holds one constant decay rate. Also over one wavelength the energy loss is considered to be constant (Yilmaz, 2001). Hence higher frequencies will lose energy more rapidly than lower frequencies. Consequently the subsurface will act as a low-pass filter (Yilmaz, 2001).

The thirdly wave attenuation phenomena is observed about viscoelasticity, meaning many earth material do not behave perfectly elastic. To calculate requires modifications to Hooke's law. This attenuation phenomenon is frequency dependent and believed to be negligible within the range of frequency for seismic prospecting acquisitions.

At stratified earth models with sharp discontinuity the seismic wave is subject to reflection and refraction. The incident wave is divided whether it is a P-wave or S-wave. This is not a transformation of wave energy, it stays the same, but are divided and have impact on how much of the initial source energy reaches the surface. How waves divide and choice of path are described further in section 2.2 and 2.2.2.

2.2.1 Snell's law

Consider a vertically layered subsurface of different rock properties. At interfaces between layers with different acoustic impedance the wave is portioned into a reflected and transmitted compressional wave and, if possible, shear wave. Acoustic impedance are discussed in section 2.2.2. Snell's law declare that the

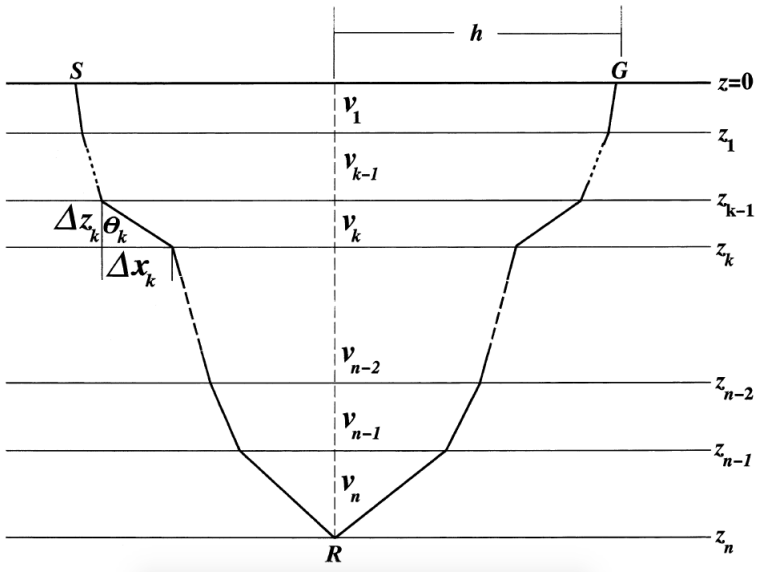

Figure 2.4: Ray trace from source to receiver in a multi-layered rock model, (Yilmaz, 2001)

angle of transmission and reflection can be calculated from the angle of incidence and velocities in the two layers,

$$p = \frac{sin(\theta_{k-1})}{v_{k-1}} = \frac{sin(\theta_k)}{v_k} \quad , \tag{2.2}$$

where $\theta_{k-1}, \theta_k, v_{k-1}$ and v_k are the incident angle, transmitted angle for the, top layer velocity and bottom layer, k, velocity of the interface.

With support from figure 2.4 half the source-receiver offset [2] can be calculated from

$$h = \sum_{k=1}^{n} tan(\theta_k)\Delta z_k \quad , \tag{2.3}$$

Also

$$tan(\theta_k) = \frac{pv_k}{\sqrt{1 - p^2 v_k^2}} \tag{2.4}$$

and

$$\Delta z_k = \frac{v_k \Delta \tau_k}{2} \quad , \tag{2.5}$$

[2] See glossary in appendix A.

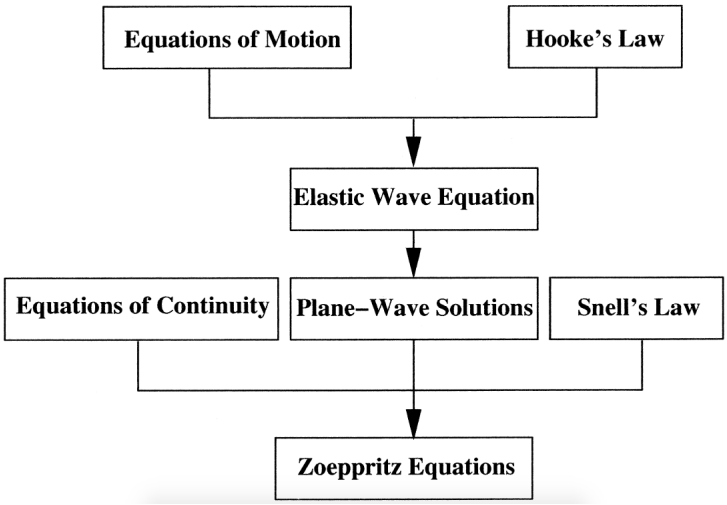

Figure 2.5: Schematic principle of how the Zoeppritz equations are derived, (Yilmaz, 2001)

where τ_k is the two-way time for the kth layer. After substitution of equation 2.4 and 2.5 into 2.3 where $2h = x$ yields

$$x = \sum_{k=1} n \frac{p v_k^2 \Delta\tau_k}{\sqrt{1 - p^2 v_k 2}} \quad . \tag{2.6}$$

Hence equation 2.6 gives the full source-receiver offset as shown from S to G in figure 2.4.

2.2.2 Zoeppritz

The Zoeppritz equations are describing how an incident P-wave is divided into transmitted and reflected P-waves and S-waves. From Snell's law the refracted and reflected wave angles are calculated for both P-waves and S-waves. By substitution into the Zoeppritz equations the amplitudes are computed.

The derivation of the Zoeppritz equations will not be done here. Detailed derivation can be found in *"Seismic data analysis"* by Ö. Yilmaz or a simpler principal guidance can be found in *"An introduction to geophysical exploration"* by P. Kearey et.al. One schematic principle of how the derivation are done are shown in figure 2.5. Zoeppritz equations require the incident P-wave amplitude and angle together with the reflection and refraction angles. From the incident P-wave, compressional wave, both compressional and shear waves splits up into reflected and refracted waves, illustrated in figure 2.6.

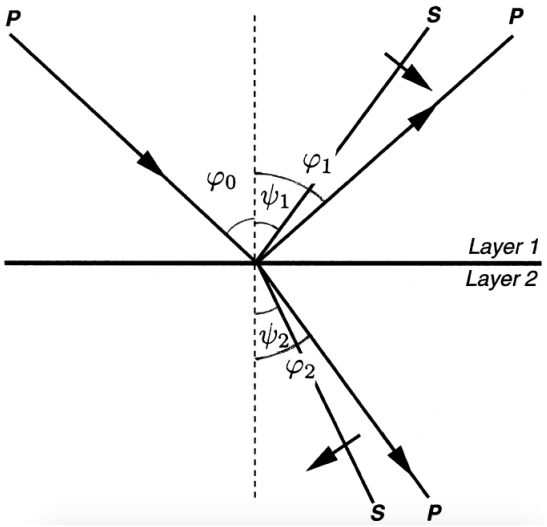

Figure 2.6: Incidence compressional wave partitioned into reflecting and transmitting compressional (P) and shear (S) waves, (Yilmaz, 2001)

An extended relationship of Snell's law from section 2.2.1 are presented in equation 2.7. All the angles that can be computed from the relationship in equation 2.7 are necessary to be able to pursue to the Zoeppritz equations.

$$\frac{sin(\varphi_0)}{\alpha_1} = \frac{sin(\varphi_1)}{\alpha_1} = \frac{sin(\varphi_2)}{\alpha_2} = \frac{sin(\psi_1)}{\beta_1} = \frac{sin(\psi_2)}{\beta_2} \tag{2.7}$$

where $\alpha_1, \alpha_2, \beta_1, \beta_2$ are the compressional wave velocities in top and bottom layer, shear wave velocities in top and bottom layer and $\varphi_0, \varphi_1, \varphi_2, \psi_1, \psi_2$ are the angles for the incident compressional wave, reflected compressional wave, transmitted compressional wave, reflected shear wave and transmitted shear wave. Substitution into the Zoeppritz equations, the reflecting and refracting amplitudes can be solved. For this case the equations have been normalized by the incident wave equal to 1, or can be considered 100 percent.

$$cos(\varphi_1)A_1 + \frac{\alpha_1}{\beta_1}sin(\psi_1)B_1 + \frac{\alpha_1}{\alpha_2}cos(\varphi_2)A_2 - \frac{\alpha_1}{\beta_2}sin(\psi_2)B_2 = cos(\varphi_1) \tag{2.8}$$

$$-sin(\varphi_1)A_1 + \frac{\alpha_1}{\beta_1}cos(\psi_1)B_1 + \frac{\alpha_1}{\alpha_2}sin(\varphi_2)A_2 + \frac{\alpha_1}{\beta_2}cos(\psi_2)B_2 = sin(\varphi_1) \tag{2.9}$$

$$-cos(2\psi_1)A_1 - sin(2\psi_1)B_1 + \frac{\rho_2}{\rho_1}cos(2\psi_2)A_2 - \frac{\rho_2}{\rho_1}sin(2\psi_2)B_2 = cos(2\psi_1) \tag{2.10}$$

$$sin(2\varphi_1)A_1 - \frac{\alpha_1^2}{\beta_1^2}cos(2\psi_1)B_1 + \frac{\rho_2\beta_2^2\alpha_1^2}{\rho_1\beta_1^2\alpha_2^2}sin(2\varphi_2)A_2 + \frac{\rho_2\alpha_1^2}{\rho_1\beta_1^2}cos(2\psi_2)B_2 = sin(2\varphi_1) \quad (2.11)$$

Equation 2.8 to 2.11 gives the Zoeppritz equations where A_1, A_2, B_1 and B_2 are the unknown amplitudes for the reflected P-wave, refracted P-wave, reflected S-wave and refracted S-wave to be solved. Also rho_1 and rho_2 are the density of the top and bottom layer. This set up of equations enables A_1, A_2, B_1 and B_2 to be computed while consider the inclination P-wave to be 1, i.e. 100 percent, thus only coefficients are computed. When not knowing the densities of the layers they need to be estimated. Predictions on how the P-wave velocity related to the density is called the Gardner's rule and is expressed accordingly (Gardner et al., 1974)

$$\rho = 0.31v_p^{0.25} \quad (2.12)$$

When solving the equations the reflection and refraction angles together with density and velocities of the top and bottom layers must either be computed or estimated. For a simulated model this is not a problem while the densities and velocities are given.

2.3 Seismic acquisition

Acquiring seismic data are done by surveys at various places with very different conditions; i.e. in the dessert, in the jungle, at the seafloor, as towed continuously in the water. Simplified the acquisition can be made at land or at sea. The principle is the same but differences exist and this report will focus on the acquisitions made through towing equipment from a vessel in a marine environment. Marine surveys are often carried out by a special made vessel going in certain patterns while towing a set up of equipment. Dependent on the target of the survey the set up of equipment are different. For the usual case the target objective are deep down in the subsurface, several kilometres deep.

The parlance is for most occasions "seconds of depth" instead of talking in terms of meters of depth. Using seconds is due to meters of depth involve some kind of velocity interpretation because the recorded data are measured in seconds. While deep target surveys are performed to discover natural resources these acquisitions covers most of the areas of interest.

To accomplish a typical deep target seismic survey acquisition the typical basic set up are modified accordingly. One special made vessel are towing a source

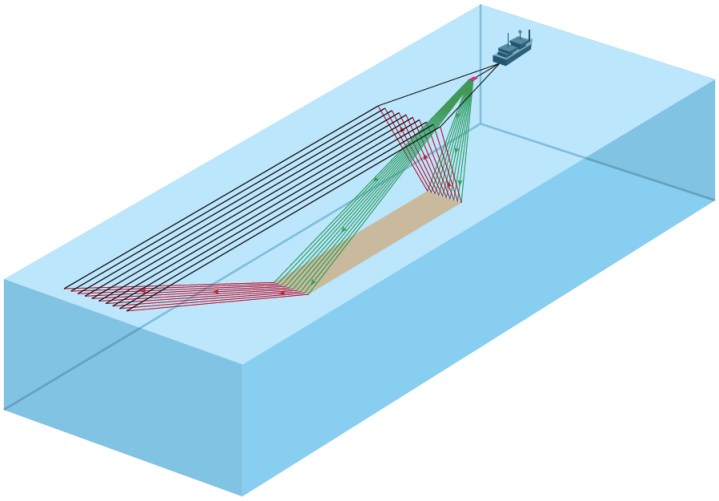

Figure 2.7: Illustrating the geometry of a conventional survey. Green lines are describing down going seismic waves, while red lines indicate up going seismic waves. Black lines show the receiver hydrophones equivalent spaced along cables, i.e. streamers. The brown area marks one reflecting level. (Brice et al., 2013)

and receivers a few meter below the water surface. The source is often composed of coupled airguns. The receivers detecting seismic waves reflected in the subsurface are hydrophones only identifying compressional waves. Typically the hydrophones are positioned to enable processing of 3D spatial imaging. Towed in parallel kilometre long lines the hydrophones are spaced with 12.5 or 25 meter. About 10 parallel lines are common but are shifting a lot. When acquiring data the source is released with equal distance, for instance every 50 or 100 meters. The seismic energy released holds carefully modified characteristics such as amplitude and frequencies. The earth more rapidly absorbs higher than lower frequencies. Hence deep seismic surveys focuses on creating energy in the low frequency spectra. However high frequencies exist even for these surveys (Selvage et al., 2012).

2.3.1 Azimuth

The essence in the concept of azimuth is to enable 3D spatial imaging of the subsurface. The concept is to have receivers in more than one direction from the source. Consider a straight line after the survey vessel and a receiver an arbitrary distance aside from the survey line, the angle at the source between the receiver and the survey middle line are forming an azimuth. Commonly sail lines

Figure 2.8: Illustration the meaning of azimuth. Image changes with the relation of direction between the spoon and irregularity of the glass. From the left the spoon is fully visible, distorted in the middle and invisible to the right. (Brice et al., 2013)

are straight parallel lines over the survey area (Brice et al., 2013). Acquisitions without azimuth are carried out by a vessel towing a source followed by one single line of receivers sailing in straight parallel lines.

The precariousness concerning single line non-azimuth is the risk of being unable to image certain anomalies. During surveys significant distance occurs between two sail lines, otherwise the progress of the acquisition would be to small. The risk would then be the lack of coverage in between sail lines. A second risk is that anomalies appear parallel along the sail lines. Parallel subsurface anomalies are very hard to image and therefore hard to distinguish in a processed seismogram. These single line set-ups are often the case for high definition surveys targeting shallow subsurface objectives.

Figure 2.8 illustrates the effect of an azimuth and non azimuth survey. Consider a fracture zone then the spoon to the left visualizes how the fracture zone is detected perpendicular to the sail lines. For this case an azimuth survey as well as a non-azimuth would detect the anomaly. The two spoons two the left would then represent the fracture zone going parallel along the sail lines. For the single line non-azimuth survey the imaging would be something like the picture to the right. The spoon is not visible. For an azimuth survey parallel to the fracture zone the spoon in the middle would be illustrative.

2.3.2 Resolution

Seismic imaging is an important tool in the industry of searching for natural resources. Recorded measurements are processed to interpret the earth's subsurface as accurate as possible. For this purpose it becomes interesting how small structures can be imaged. Resolution is about how close two individual

seismic measured events can be distinguished. Resolution are dependent on the survey set up. Vertical and lateral resolution are expressed differently however both relates to the dominant frequency (Yilmaz, 2001). While the dominant frequency usually decreases with depth so does resolution (Kearey et al., 2002).

Vertical resolution is defined as if two reflections from top and bottom of a thin layer are separable, mainly dependent on dominant wavelength (Yilmaz, 2001). For seismic waves the dominant wavelength is given by

$$\lambda = \frac{v}{f}, \tag{2.13}$$

where f is the dominant frequency and v is the seismic propagation velocity. Intuitively Compaction of the subsurface increases with depth. Hence velocity often increases with depth due to compaction. Ordinary propagation velocities for the subsurface are in the range about 2000 m/s to 5000 m/s (Yilmaz, 2001). As described in section 2.2 lower frequencies becomes more prominent with depth. Conventional surveys are often configured with lower dominant frequencies while dedicated 2D high resolution surveys are designed for higher dominant frequencies (Yilmaz, 2001).

The definition of resolution is that "reflections from the top and bottom of a thin bed are seen as separate events or wavelet lobes" (Yilmaz, 2001). For two events to be separable $\frac{1}{4}$ of the dominant wavelength is often a threshold, λ, but can also be smaller (Yilmaz, 2001). To resolve a thin layer is strictly speaking not the same to map it. Even if two events are not properly separated it can still be mapped, distinguished as two events. For one particular layer the conditions for mapping are different depending on the circumstances. Depending on noise and how the amplitude of the reflection stands out the mapping conditions are often between $\frac{1}{4}$ and $\frac{1}{16}$ of the dominant wavelength, λ (Yilmaz, 2001). When mapping gas occurrences amplitude analysis can be a useful method. Mapping by changes in amplitude often helps detecting layers below the resolution limit, thus events are not strictly separated.

$$MDL = \frac{\lambda}{\Omega} \tag{2.14}$$

where MDL is the minimum detectable layer, λ is the dominant wavelength and Ω is an unitless integer probably between 4 and 16. Ω is the fraction of a wavelength that can detect a layer. Four plots, figure 2.9 and 2.10, are presented of how minimal detectable layer relates to frequency and velocity. The x-axis are frequency variation, the almost parallel plotted curves within the same figure are representing different velocities for the minimum detectable layer on the y-axis. Section 2.3.2 is presenting how the subsurface are resolved. A rule of thumb is that a threshold for resolving a layer properly is the layer thickness

should not be thinner than the wavelength divided by 4, but realistically more thin layers could be resolved.

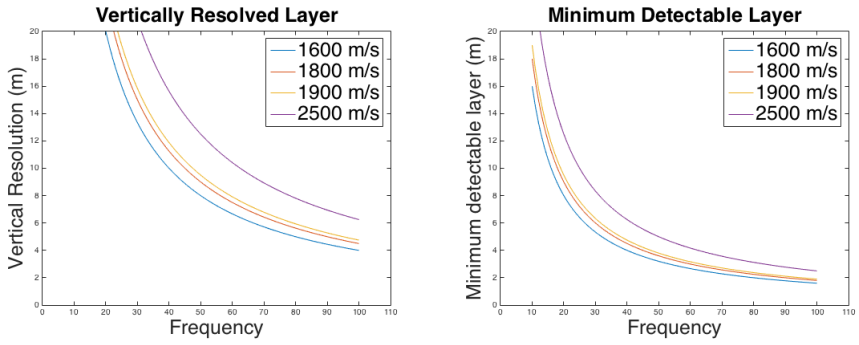

(a) (b)

Figure 2.9: Vertically resolved and minimum detectable layer for different propagation velocities, from top: 2500, 1900, 1800 and 1600 m/s. (a) Vertically resolved layer based on $\frac{1}{4}$ of the dominant wavelength (Yilmaz, 2001). (b) Minimum detectable layer based on $\frac{1}{10}$ of the dominant wavelength (Yilmaz, 2001).

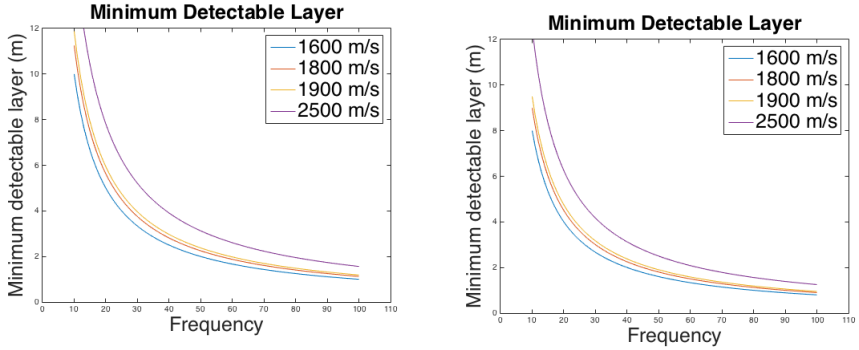

(a) (b)

Figure 2.10: Minimum detectable layer for different propagation velocities, from top: 2500, 1900, 1800 and 1600 m/s. Minimum detectable layer based on $\frac{1}{16}$, (a), and $\frac{1}{20}$, (b), of the dominant wavelength (Yilmaz, 2001).

Horizontal resolution is related to the same principle as vertical resolution but instead for the horizontal plane. Yet the theory behind is expressed as more than a ratio of the wavelength. The horizontal resolution is mainly a result by two controls. One is the horizontal spacing of the detectors, which is crucial, another the physical behaviour of the seismic waves. Hereby will focus on the latter physical intrinsic. The theory explaining horizontal resolution is known as the Fresnel zone. The cross section of a spherical seismic wave propagation illustrates the Fresnel zone in figure 2.11. Consider a coincident source and

reflector point above a flat horizontal reflector. The two way time for the energy from the source point, S, to the reflection point, O, and back to S is given by

$$t_0 = 2\frac{z_0}{v}, \tag{2.15}$$

where z_0 is the metric distance and v is the propagating velocity. Let the spherical propagation front be followed up by a sphere at $\frac{1}{4}$ of a wavelength later. When the second sphere reaches the reflector at point O the first sphere circles an area of the reflector plane called a half-wavelength Fresnel zone (Yilmaz, 2001). This is shown in figure 2.11 for a cross section and is denoted by A and A'. The two way time for the reflected energy from the source S to A, or A', and back to S is given by

$$t_1 = 2\frac{z_0 + \frac{\lambda}{4}}{v}.$$

The energy reflected within the Fresnel zone will be encapsulated by the time step $t_1 - t_0$ and generally considered indistinguishable. The horizontal resolution is strictly defined by the reflection of the half-wavelength Fresnel zone. Where the threshold for being resolved is given by the zone's radius

$$r = \sqrt{\frac{z_0\lambda}{2}}. \tag{2.16}$$

Where equation 2.13 and 2.15 substituted into 2.16 gives the radius expressed

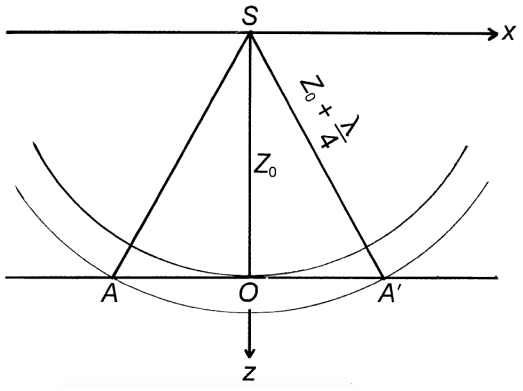

Figure 2.11: How the Fresnel zone is spreading as a disc and how it relates to the vertical resolution, $\frac{1}{4}\lambda$. S is coincident source and receiver point, Z_0 is reflection at zero source-receiver offset, AA' is defining the Fresnel zone (Yilmaz, 2001).

accordingly

$$r = \frac{v}{2}\sqrt{\frac{t_0}{f}} \tag{2.17}$$

2.4 Processing

Data acquisition from an area of interest is always followed by a processing flow. All managing of the data is called processing. The processing flow can be very different depending on what should be achieved or whom is doing the processing. One and the same processing flow can also be described in different ways. Here will be presented, in figure 2.12, one processing flow in general terms applied by many. Many other features are often added to the process but any of the presented steps are rarely taken away. Figure 2.12 illustrates this general processing flow (Hatton et al., 1996).

Under each step in the flowchart, illustrated in figure 2.12, hide parts which all together form the sort of formatting in the step one seeks. The formatting are often applied to the data set by programmed algorithms. Algorithms used by commercial processors are kept a secret but are building on the same mathematical foundation. The different steps in figure 2.12 are foremost meant to illustrate the schematic sections of a general processing sequence, rather than explain it. The first step, "Input seismic", is to load the data into a software. This can often be a challenging task. For the second step, "gather", the reader is referred to the glossary in appendix A. The third, fourth and fifth step is normal moveout correction (NMO), mute and stack, which is described below in section 2.4.1 and 2.4.4. The last and sixth step is displaying, which means that the software is displaying a gather of the data. Displaying in it's simplest form is what has been done in figure 5.2 to 5.13. The subsidiary step, "Velocity analysis", is a computation or estimation of the seismic wave propagation velocity of the subsurface layers. The velocity analysis is important to anticipate the normal moveout corrections, to be able to make the computations.

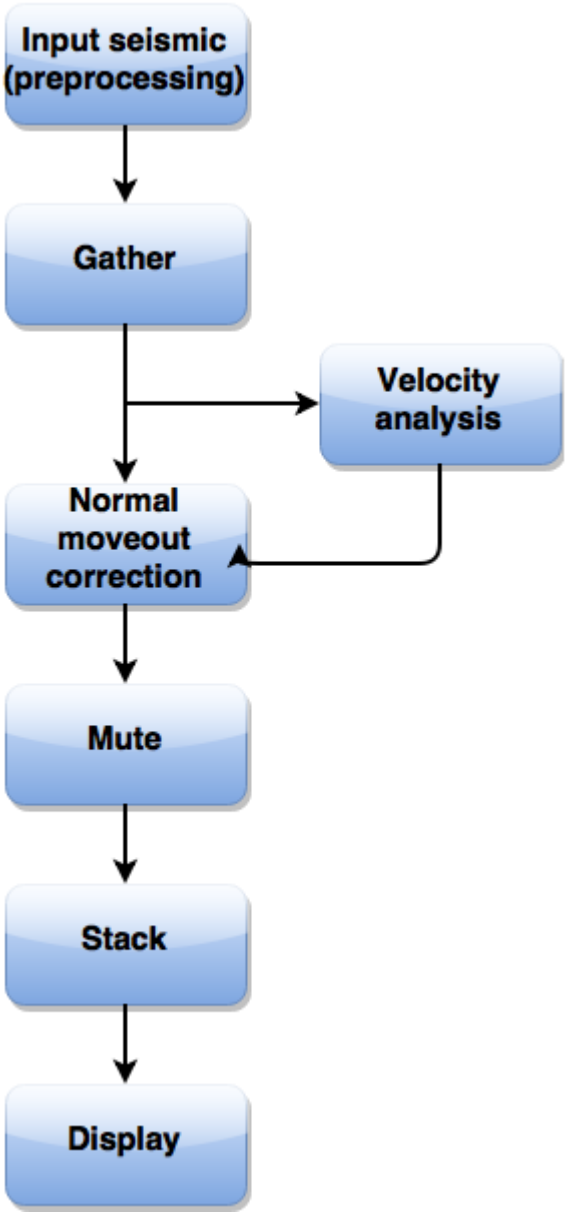

Figure 2.12: Typical processing sequence, (Hatton et al., 1996). General descriptions for input seismic, dispaly and velocity analysis can be found in this section, for gather see appendix A, for normal moveout correction, mute and stack see section 2.4.1 and 2.4.4.

2.4.1 Normal Move Out

Consider a single horizontally flat interface between two layers with contrast in acoustic impedance. Reflected seismic waves will then arrive and appear as an hyperbola when plotted. Intuitively the signal is recorded later for every receiver away from the source. This is called *normal move out* (NMO) and the hyperbola is more flattened for every deeper interface. The travel time from the source down to the reflecting point, *mid point*, and up to the receiver are computed by the Pythagorean theorem as a function of source-receiver offset [3].

$$t^2 = t_0^2 + \frac{x^2}{v^2}, \tag{2.18}$$

where t is the travel time from the source to the receiver, t_0 is twice the vertical travel time from the surface to the mid point, x is the distance (offset) and v is the velocity of travelled path. To restore signals corresponding to the reality the NMO needs to be corrected. The NMO correction, Δt_{NMO} are the difference between the t_0 and t

$$\Delta t_{NMO} = t - t_0. \tag{2.19}$$

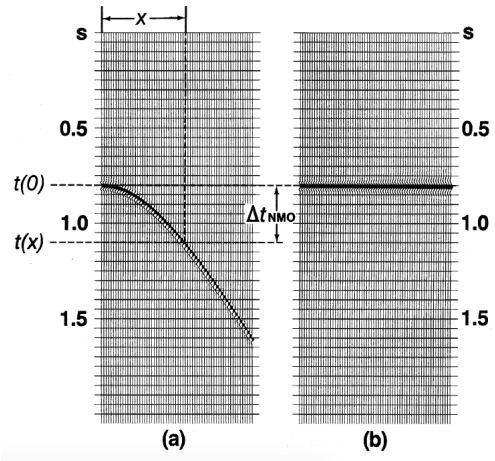

Figure 2.13: Illustration of how acquired data from a flat reflector forming an normal move out hyperbola (a) are corrected to it's corresponding vertical travel time (b) (Yilmaz, 2001).

[3] See glossary in appendix A.

Where equation 2.18 substituted into 2.19 yields

$$\Delta t_{NMO} = t_0 \left[\sqrt{1 + \frac{x}{v_{NMO} t_0}^2} - 1 \right]. \tag{2.20}$$

To stack [4], somehow normalize, the acquired traces to a *common mid point* [5] (CMP) gather [6] must be preceded by a NMO correction (Yilmaz, 2001). When implementing a NMO correction the traces are usually stretched with receiver offset and also more severe at the shallow parts. Stretch is called when the wavelet is elongated to range over a longer period of time. Normally the stretched data are unusable and needs to be taken away by a mute [7]. This depends on how severe the data is stretched. Figure 2.13 illustrates how each trace are corrected into the corresponding position for the vertical travel time to a flat reflector with very little stretch.

2.4.2 Multiple attenuation

Seismic surveys acquire all types of seismic waves primary reflections as well as head waves from refractions, noises from the surrounding and multiple reflections. This section will focus on primary and multiple reflections. *Primary reflections*, or *primaries*, are seismic waves reflected (upwards) only once on its path from source to receiver. In a stratified subsurface some of the energy reaching the receiver at the surface have been reflected more than once on it's way down, up or both. Normally these *multiple reflections*, or *multiples*, are considered to be noise and attenuated from the seismic data (Verschuur, 2006). For most cases primaries have higher amplitudes than multiples due to energy loss for each reflection. However two types of multiples tend to have significant high amplitudes comparable to primaries: ghost reflections and water layer reverberations (Kearey et al., 2002). Figure 2.14 illustrates how seismic waves will behave in different ways and create multiples.

In general there are two categories of multiple reflection attenuation techniques used (Verschuur, 2006)

- "methods based on a difference in spatial behaviour of primaries and multiples"
- "methods based on a periodicity and predictability".

[4] See glossary in appendix A or section 2.4.4.
[5] See glossary in appendix A or section 2.4.4.
[6] See glossary in appendix A.
[7] See glossary in appendix A.

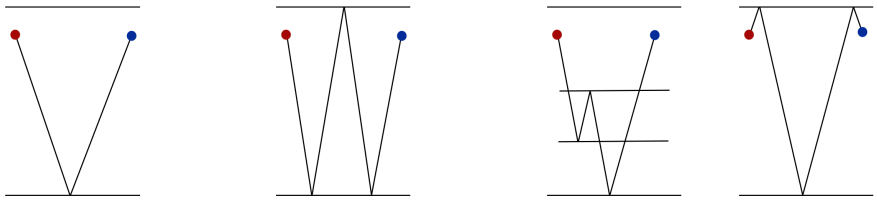

(a) (b) (c) (d)

Figure 2.14: (b) to (d) are sketches of ray paths for various multiple reflection types. Source to the left, receiver to the right. Upper line represent water surface and first lower line the seabed. (a) primary reflection, (b) water bottom reverberations, (c) pegleg reflections, (d) ghost reflections.

The first category is based on how multiples bounces in shallower subsurface yet arrives at the approximately the same time to one receiver as a primary. Multiples have by nature taken a shorter subsurface path in a slower propagating media than a primary. The primary's path is deeper hence propagated in faster media, i.e. more consolidated rock at greater depths. Differences in the propagation environments will be shown considering several receivers. Consequently the normal move out (NMO) will be different for the multiple and primary recordings. In a secondary stage, during the NMO correction, these multiples will distinguish themselves if velocity picking is done correctly (Verschuur, 2006).

The second category is based on predictions of statistics. Multiple reflections have an inherent relationship to primaries. The simplest form of multiple appears in a repetitive pattern. For more complex cases predictions of the multiples are made by connecting the primaries to the wave equation and compute the multiples, match them to the real data set and suppress them. To make computations and supress, assumptions need to be done, i.e. the earth model. These methods are preferably used in the pre-stack [8] domain but can with simplifications be performed in the post-stack or post-migration stage.

2.4.3 Frequency filtering

Normally frequency filtering is carried out during processing. Consider seismic data in the frequency domain. The aim of frequency filtering is to preserve targeted bandwidth and suppress rejected frequency spectra. This can be done to with intention to cut off low or high frequencies. Viewed upon contrary is that a high bandwidth cut off is a passed low spectrum. Hence the expressions

[8] See glossary in appendix A.

low-pass and high-pass filter. If a bandwidth within certain limits is requested the frequencies outside are cut off, applying both low-pass and high-pass filters. This is called band-pass filter.

The aim for designing band-pass filters is to pass a certain bandwidth without harm to the passed signal and suppress the cut off spectrum to desired result. Mathematically this is illustrated by

$$A(f) = \begin{cases} 1 & f_1 < x < f_2 \\ 0 & \text{else} \end{cases}$$

where A is the amplitude at a certain frequency in the frequency domain and f_1 and f_2 gives the band-passed limits. This is also referred to as the boxcar. Ideal boxcar would form a rectangle by determining frequency limits and maximum amplitude. As illustrated in figure 2.15 (a) vertical limits causes ripples in the cut off frequencies. While some frequencies are being suppressed others are amplified. This is called Gibbs phenomenon. Creating a band-pass with frequency limits as slopes circumvents this. In figure 2.15 (c) the ripples are almost gone, where A, B, C and D are corner frequencies for this type of trapezoid band-pass. For further reading on the subject please read *Seismic data analysis: processing, inversion, and interpretation of seismic data* by Yilmaz.

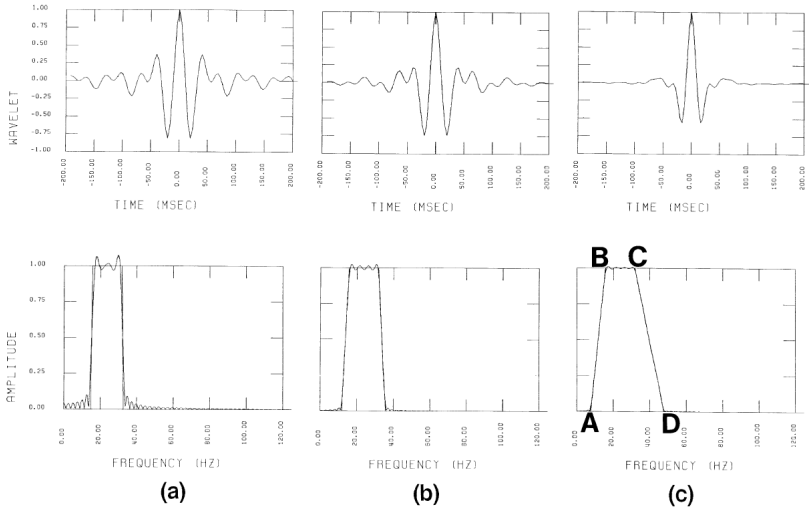

Figure 2.15: The top row represent zero-phase wavelets and the bottom row the corresponding amplitude spectra. (a) show a band-pass of almost vertical limits, which creates ripples. The ripples attenuate with a moderate slope (b) and even more with greater slope (c). In (c) A, B, C and D represent the corner frequencies. (Yilmaz, 2001)

2.4.4 Stacking, common-mid-point and mute

Stacking and muting can be performed in several ways. To establish a general mathematical method for how most are performing stacking and muting is hard. Therefore the principals for what is achieved will be described.

To start with stacking; for marine acquisitions stacking is often performed for common-mid-points (CMP). To understand CMP-stacking it is crucial to understand the concept of CMP. A CMP is the reflecting point for a seismic ray, for this case with flat reflectors the CMP is midway between the source and receiver along the sail line. While the coordinated for a CMP is constant, the position for the source and receiver will change. Consequently one single CMP will reflect several rays spaced in time. Figure 2.16 illustrates the concept of CMP. In the processing stage the overlapping CMP traces are sorted to each corresponding CMP coordinate. This process of adding the traces to a vicinity of one coordinate, called bin, and normalize such as amplitude to a single trace. Different methods performs normalization and weighting of traces differently.

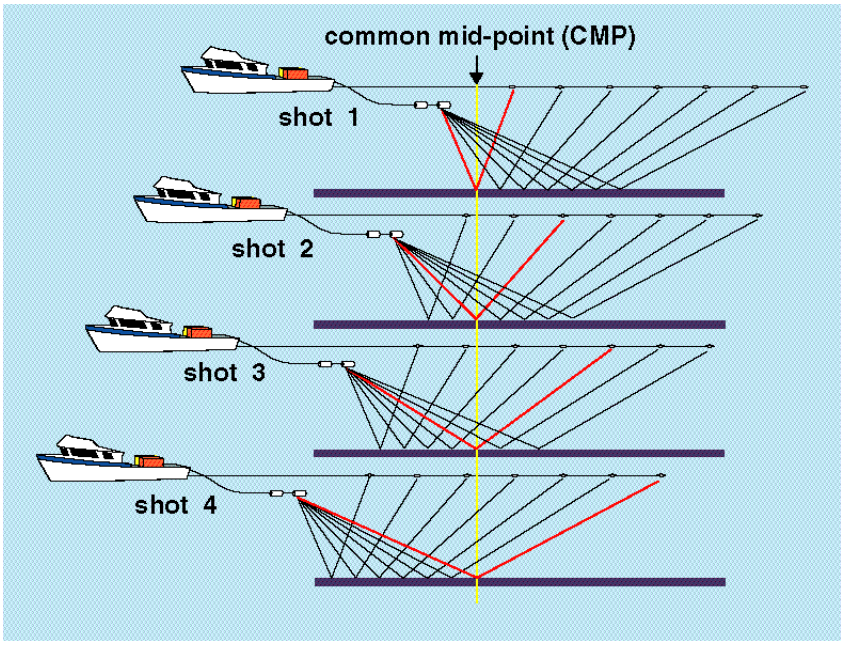

Figure 2.16: Visualisation of the common-mid-point (CMP) concept, (U.S. Geological Survey, 2001). The four vessels illustrates one vessel releasing it's source at different locations along a sail line. For one reflecting CMP the ray paths becomes longer with source-receiver offset.

Secondly muting is also part of the processing sequence. Muting is simply data subtracted. The data subtracted are often selected from a gather [9] or stack, which are considered not to contribute accurately. One common underlying cause to muting is the stretch, i.e. incorrectness, of the traces arise with source-receiver offset when applying a NMO correction. More about NMO correction can be read about in section 2.4.1. Mute can be applied solely by a computer algorithm but are often picked by hand. A usual case would be for an interpreter to pick a polygon on a displayed stack or gather from which the algorithm applies the mute. Before and after a simple mute is illustrated in figure 2.17. The effect of a mute for a real case data are also illustrated in the differences between figure 5.14, to which no mute is applied, and figure 5.15, to which mute is applied.

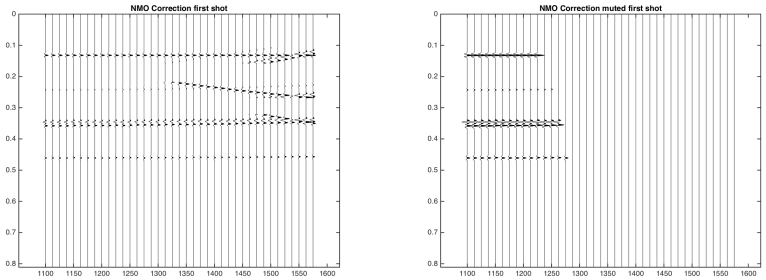

(a) (b)

Figure 2.17: The left subfigure (a) display a gather after NMO correction has been applied. Some of the data in the subfigure is still considered not to contribute to an accurate imaging and therefore a mute is applied. The right subfigure (b) display the same gather after a mute has been applied. The mute was applied as a straight line. An angle of the mute line and position was also determined by hand, not by a computerised algorithm. The units on the X- and Y-axises are neglected in this figure.

[9] See glossary in appendix A.

CHAPTER 3

HIGH DEFINITION

Conventional 3D seismic surveys for exploration purposes are designed for image geological structures several kilometres beneath the subsurface. Hence conventional imaging of the shallow sub seabed does not give a satisfactory resolution. This is one of the reasons to why dedicated high resolution surveys are acquired to image the shallow sub seabed. As resolution decreases with higher propagation velocity and lower frequency, dedicated high resolution surveys are designed to have a high dominant frequency relative to conventional deep target surveys (Blaauw et al., 2012). Conventionally processed 3D exploration 3D surveys may have about 12 m of vertical resolution in the shallower sediments, i.e. upper hundred meters, while a dedicated high resolution survey may resolve a 5 meter layer (Blaauw et al., 2012).

High definition images are needed in a late stage in the exploration development cycle. The first stages of a typical exploration/production cycle is illustrated in figure 3.1 to give a sense of when the high definition is needed. The cycle starts with a government license for exploring oil and gas. It goes on to conventionally acquire deep target 3D data, described further in section 2.3. The acquired data are then processed for a deep target such as large reservoirs of oil and gas, briefly explained in section 2.4. The processing generates a display of the estimated subsurface. The subsurface is then interpreted and in the next prospecting-stage is where the oil and gas reservoirs are predicted to exist. If any reservoir worth recover was predicted then a prospect is set up. Here in the "well placement"-stage the shallow subsurface is still unknown and a borehole is placed close to the predicted reservoir. The borehole placement is supposed to be corrected to a more suitable spot avoiding geohazards in an iterative process. Further about

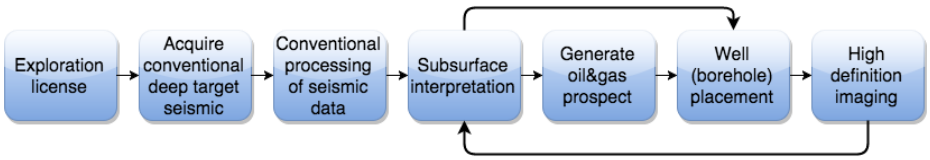

Figure 3.1: Schematic stages in an exploration development cycle to give a sense to when, in the bigger perspective, a high definition image is needed. For the different stages see text above.

geohazards and geohazard predictions can be read in section 3.2. The stage "high definition imaging" involves here both reprocessing of conventional deep target 3D data and acquiring as well as processing dedicated high definition data. This report is an evaluation of reprocessed conventional 3D data for shallow subsurface interpretations and is further explained in section 3.2. From the high definition imaging stage it goes back to the subsurface interpretation stage to identify geohazards and later adjusting the borehole placement from geohazards.

3.1 Geohazard predictions

In an marine environment with hundreds up to thousands of meters to the seabed, the conditions of the seabed and below are unknown. There are several reasons why investigations of this region below the seabed are a necessity. With these uncertainties it is of interest to investigate and quantify the risk associated with geohazards. One definition of geohazards is "a geological state, which represents or has the potential to develop further into a situation leading to damage or uncontrolled risk" (Vanneste, 2010). Techniques for high definition interpretation of the shallow submarine part are foremost driven by the petroleum industry. Due to big investments and authority regulations risk assessments are required. Geohazardous failure scenarios will effect field installations or third party assets due to geomechanical failure modes. Therefore geohazard identification investigates geological occurrences that may lead to some failure scenario triggered by (Nadim and Kvalstad, 2007)

- "bathymetry and seabed gradients (sedimentation, erosion)"
- "pore pressure conditions/fluid flow"
- "soil strain-softening under increased static and cyclic loading"
- "generation of fluid/gas flow under or close to foundations"

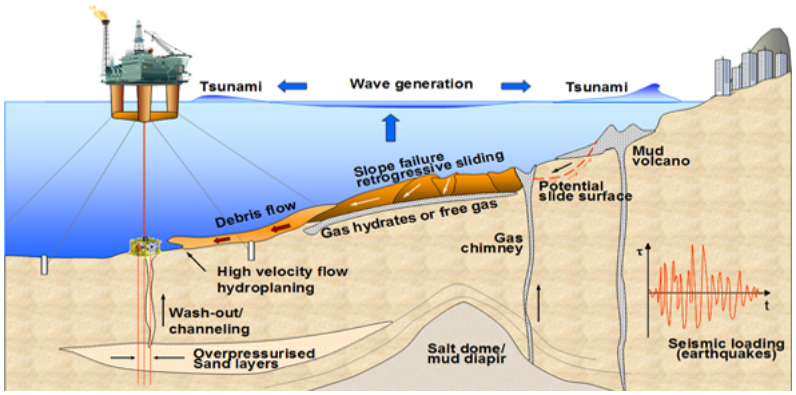

Figure 3.2: Selection of possible offshore geohazards (Vanneste, 2010)

- "temperature increase around wells, manifold structures and pipelines causing gas hydrate melting followed by gas bubble expansion, fracturing and free water that will reduce the shear strength of the soil"
- "cratering caused by blow-outs/uncontrolled gas and shallow water flow".

Figure 3.2 illustrates some of the potential geohazards that need to be under consideration during offshore risk assessments. Before putting big structures at the sea floor a risk minimisation needs to be done. Due to authority requirements but also foremost the devastating consequences a missed identification of a geohazard can have putting human lives at risk it is important. When investigating the subsurface imaging an interpreter is looking for anomalies that stand out such as spots or lines with high contrast in amplitude.

3.2 High definition from conventional data

High definition surveys are normally achieved by acquiring dedicated high resolution survey data. As proclaimed in section 2.3.2 the resolution are dependent on velocity and frequency. While the velocity of the investigated subsurface can not be controlled the frequency content of the survey is important. Dedicated high resolution surveys are designed to have a frequency spectra in the higher end. Conventional acquisitions are designed for deep targets hence the dominant frequency is lower. Nevertheless conventional surveys concurrently carry high frequency data. The high frequency content of conventional surveys are inferior to that of dedicated high resolution surveys which is why the complementary surveys are performed (Blaauw et al., 2012). However dedicated high resolution 2D surveys lack in two areas compared to conventional surveys (Blaauw et al., 2012):

- To map thicker layer also lower frequencies are required in addition to the high frequency bandwidth that are the case for dedicated high resolution site surveys.
- For an better spatial imaging and understanding of the geology investigated 3D data coverage are important which is not the case for 2D surveys even if the acquisition lines are close.

By changes in the processing flow of the conventionally acquired data high definition imaging can be achieved. This has been proven successful in identifying geohazards at deepwater fields greater than 500 meters (Blaauw et al., 2012). Outcome of the high definition processing at appropriate deepwater sites the Norwegian Saftey Authorities have accepted the processing sequence as alternative for dedicated 2D high resolution surveys (Blaauw et al., 2012).

To start with the new high definition processing only uses traces at near receiver offsets carefully selected from the conventionally acquired 3D data. Figure 3.3 illustrates crucial stages that are partially iterated for the high definition imaging. First static correction need to be done with great care. While the target of the high definition imaging are close to the survey vessel, source and streamer static data differences is of great impact. By carefully performing static [1] correction acquisition footprints [2] can be reduced. The second stage of demultiple is new to high definition reprocessing. This is because shallow high definition imaging has not successfully been reprocessed before, for conventional shallow water deep target 3D acquisitions. The principles of demultiple are explained in section 2.4.2. In the last stage, interpolation, are performed to de-alias the image, i.e. taking away the fish bone pattern, and by doing so intelligently both the temporal and spatial resolution are preserved. Interpolation means gaps are filled or improved based on 5 parameters; azimuth [3], dip [4], crossline [5], inline [6] and geophone offset [7].

In high definition processing of conventional deepwater 3D surveys only the data above the arrival times of the first water bottom multiple are used. This makes deepwater acquisitions suitable for shallow sub seabed imaging. This shallow high definition processing for data sets acquired at deep water have been made before. The new challenge is when multiples emerge for shallow water acquisitions and consequently increases the pressure on multiple attenuation success. The focus of this study is on evaluating the success of the high definition processing sequence for shallow water acquired data.

[1] See glossary in appendix A.
[2] See glossary in appendix A.
[3] See section 2.8.
[4] See glossary in appendix A.
[5] See glossary in appendix A.
[6] See glossary in appendix A.
[7] See glossary in appendix A.

Figure 3.3: Crucial part of reprocessing sequence for high definition flow of conventionally acquired 3D data. For static correction see appendix A. The principles of demultiple are explained in 2.4.2. The nature of interpolation is expected to be known but how the interpolation is effecting the imaging is explained in this section.

3.3 Acquired data

Two overlapping data sets have been used for processing. One conventionally acquired narrow azimuth streamer 3D exploration survey. It has been processed conventionally and by the high definition processing sequence. The second one is a dedicated 2D high resolution site survey. The fact that the two data sets are overlapping is interesting. The opportunity opens up to compare not only imaging of a conventionally against a high definition sequence but also high definition sequence against dedicated 2D high resolution imaging. The conventional 3D survey have been acquiring data over a very large area, from which data of a smaller area has been extracted. The new processed image have a horizontal area of about 300 square kilometre, e.g. shown in figure 5.40 in the results chapter 5. The dedicated high resolution 2D survey are acquired over a smaller area with a inline [8] shift of 45 degrees angle, which is cut off and processed as a square, e.g. seen in figure 5.41 in the results chapter 5. Thus there are two surveys and three processed volumes, the conventional deep 3D survey are conventionally processed as well as processed for shallow high definition.

Figure 3.4 illustrates conventional 3D exploration survey. The acquisition parameters are accordingly. Starting with the source it is an airgun array of 4450 cubic inches and are released every 50 meters. The streamer length is 6000 meters with 480 channels spaced 12.5 meters. Streamer depth is 6 meters and the nearest receiver offset are 182 meters. Traces are recorded up to 8.2 seconds from the source release, with sampling interval of 2 milliseconds.

Figure 3.5 illustrates dedicated 2D high resolution survey. The acquisition parameters are accordingly. Starting with the source it is an airgun array of 4 times 40 cubic inches and are released every 6.25 meters. The streamer length is 600 meters with 48 channels spaced 12.5 meters. Streamer depth is 3 meters and the nearest receiver offset are 96.92 meters. Traces are recorded up to 2 seconds from the source release, with sampling interval of 1 milliseconds.

[8] See glossary in appendix A.

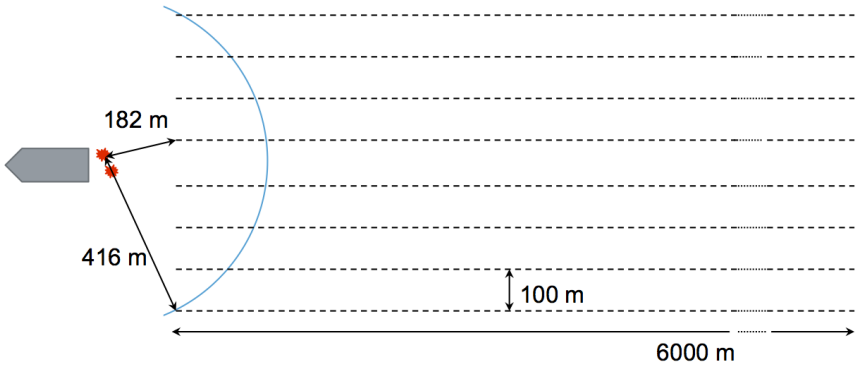

Figure 3.4: Geometry of the conventional narrow azimuth streamer 3D exploration survey set up used for acquiring the data used for high definition reprocessing. The grey "arrow" symbolises an acquisition vessel pulling 8 streamers represented by the dashed lines. The blue circle sector indicates the minimum source-receiver offset where traces are taken in account due to the heavy source load. The red stars indicates the source airgun array. This geometric illustration is viewing the set up from above. This figure do not have the same scale as figure 3.5. For a general perspective view of a conventional 3D survey see figure 2.7.

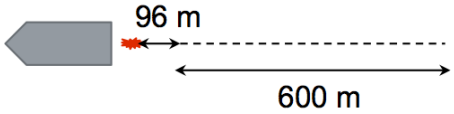

Figure 3.5: Geometry of the dedicated 2D high resolution acquisition set up used for comparable reasons, to the high definition reprocessed 3D data. The grey "arrow" symbolises an acquisition vessel pulling a streamer represented by the dashed line. The red stars indicates the source airgun array. This figure do not have the same scale as figure 3.4.

CHAPTER 4

SENSITIVITY AND INTERPRETATION INVESTIGATION

The purpose of this chapter is to explain purely what was done to achieve the results, which are analysed in a later stage. The performed stages described in this chapter are based on theory in the former chapters as well as guidance from experts at Maersk Oil.

4.1 Sensitivity investigation

The sensitivity analysis is programmed in Matlab and aims to getting an understanding of the challenges in resolve images. Computations of how the minimum detectable layer relates to frequency for different velocities were made. Minimum detectable layer where computed as equation 2.14 and displayed as graphs.

All of the computations for the sensitivity investigation, both minimum detectable layer and simulated ray tracing model, are programmed in Matlab.

4.1.1 Simulated ray tracing model

The simulated ray tracing model were set up as a vertically stratified earth model with horizontal layers, illustrated in figure 5.1. The model contained a

top layer representing water. The layers below had attributes like sedimentary rocks. The different layers were given a certain P-wave velocity. From the P-wave velocity two parameters were computed, the S-wave velocity by equation 2.1 and the density, ρ, by equation 2.12 to be able to use Zoeppritz equation properly. The layers had fixed thicknesses except for the target layer under sensitivity investigation. Two layers from the top, which of one is the water depth, were simulated 100 meters each. The three layers was totally 200 meters thick of which the middle layer was the investigated thinner layer that had various thickness from 2 to 10 meters. The last layer also had the thickness of 100 meters. The P-wave velocities from top to bottom were accordingly: 1500, 1800, 1850, v_x, 1850 and 2000 m/s. v_x is the velocity of the focused layer of which varied between the following velocities: 1800, 1900, 1600 and 2500 m/s.

Velocitymodel	1	2	3	4
Layer 1	1500	1500	1500	1500
Layer 2	1800	1800	1800	1800
Layer 3	1850	1850	1850	1850
Layer 4	1800	1900	1600	2500
Layer 5	1850	1850	1850	1850
Layer 6	2000	2000	2000	2000

From this layered earth model ray tracing was carried out with an open source code (Nainggolan, 2011) that was modified to act like a proper offshore acquisition. The ray tracing was computed as one dimensional rays from the seismic source reflected at each layer to the receivers based on Snell's law and a bisection method, equations 2.2 to 2.5. The seismic source and receivers were modelled at the sea surface and moved from the right to the left while simulating seismic source releases.

While ray tracing the two way time was computed as well as the angle of reflection. For each reflection the amplitude of the P-wave was computed by principles of Zoeppritz equation, 2.8 to 2.11, in a sub function from the Crewes (Margrave, 2006) geophysics Matlab package. Simplifications were made such that the amplitudes computed are coefficients from 100 percent inclination energy; no seismic energy was lost due to friction while propagating. Both coefficients for P-waves and S-waves were computed but only the reflected P-wave was taken in account as a primary wave. P-wave amplitude coefficients are then positioned in a matrix for it's corresponding two way time and receiver. The sampling rate was 1 millisecond. The matrix holds the maximum time divided by the sample rate as rows and the amount of receivers as columns.

The sensitivity investigation is based on how the investigated layer can be detected for different frequencies. Hence Ricker wavelets, ideal wavelets, were computed with a sub function from the Crewes package based on a range of

dominant frequencies: 30, 50, 70 and 90 Hz. All of the different wavelets were applied to all earth models with different thicknesses and velocities. For the amplitude matrix each coefficient belong to just one cell, therefore appear as a spike. These spikes were convolved with the Ricker Wavelet and created a simulated record of seismic traces.

While the velocities were known no velocity analysis were done for normal moveout correction. The normal moveout effect was corrected on basis of equations 2.18 to 2.20. For the correction algorithm the exact corresponding velocity was picked for each trace. However this does not provide a solution without error, due to difficulties in sorting crossing hyperbolas created by the traces [1]. Consequently a mute [2] was required. A straight mute line was applied from which data was cut off. The mute line was selected at an appropriate point and angle, like illustrated in figure 2.17.

Next step was to construct a stacking [3] algorithm. The traces were normalised over the number of traces added to one cell within the matrix, e.g. an average value. The traces were also arranged according to common-mid-point [4] before stacked. To display the processed image a sub function from the Crewes package was used to plot the black and white wiggles.

4.2 High definition reprocessed 3D data set

The high definition processed 3D data set's frequency spectra were investigated. This were done in the software OpenCPS [5]. Secondary interpretations of the geophysics were made in the software Petrel [6].

4.2.1 Frequency content investigation

For processing in the software OpenCPS one inline [7] of the high definition processed data were selected to investigate the frequency content. OpenCPS are structured such that selected individual processing blocks create an appropriate sequence. Each block are programed with characteristics as stages in one

[1] To see how hyperbolas are created by traces see section 2.4.1.

[2] For a description of a mute see section 2.4.4.

[3] See glossary in appendix A or section 2.4.4.

[4] See glossary in appendix A or section 2.4.4.

[5] OpenCPS is a seismic processing software, for further understanding see homepage: https://www.opengeophysical.com/

[6] Petrel is here used as an interpretation tool but have many applications, for further understanding see homepage: http://www.software.slb.com/products/platform/Pages/petrel.aspx

[7] See glossary in appendix A.

processing flow. However certain amount of input are given for the user to determine.

Four different band pass filters were applied to the inline data. Investigations were made on what impact different frequency spectra have had on imaging. First band pass filter passed low frequencies, the second were two filters that passed frequencies spectra in the middle and the fourth filter passes a high frequency spectra, relative to deep target seismic. Boxcar filter spectra were encapsulated by the frequencies:

- Low frequency spectra: 3 , 6 , 20 , 25 Hz
- Lower middle frequency spectra: 20 , 25 , 40 , 50 Hz
- Higher middle frequency spectra: 40 , 50 , 60 , 70 Hz
- High frequency spectra: 60 , 70 , 110 , 125 Hz.

To be able to stack [8] the common-mid-point [9] gathers [10] the data requires a mute [11] to generate proper images. Therefore one mute block and one block of stacking were applied to the data. The mute was set by hand as a polygon and applied by a software algorithm. The polygon was defined in a common-source gather at positions interpreted the stretch was too severe.

4.2.2 Seismic volume interpreting

Petrel was used as an interpretation tool for this master's thesis. The seismic data; conventional processed, high definition processed and 2D processed, were loaded into the software. Petrel is then able to form an inline, a crossline [12] and a horizontal pane, which are able to show an instant slice of seismic data in the three spatial directions. From these inline and crossline panes horizons, similar reflection interpreted as one layer called horizon, were picked. One horizon was picked at the seabed and the second one at a matching layer at an arbitrary depth for both the high definition processed data and the 2D data, see figure 5.21, 5.22 and 5.29. In the vicinity of the horizons attributes were extracted, such as root mean square amplitude, dominant frequency, instant frequency and two way time.

Secondary the three volumes where examined from a simple two-way-time perspective, called time slice. A time slice is a horizontal imaging of the same

[8] See glossary in appendix A or section 2.4.4.
[9] See glossary in appendix A or section 2.4.4.
[10] See glossary in appendix A or section 2.4.4.
[11] See glossary in appendix A or section 2.4.4.
[12] See glossary in appendix A.

two-way-time over the horizontal pane. For this second comparison a different colour scale was chosen, a grey scale, to be able to distinguish differences within and between the images. The Petrel tool allow the user to extract the time slices with precision of the sampling rate, which was done for all three volumes. The conventional 3D survey were acquired with a sampling rate of two milliseconds and the 2D survey with a sampling rate of one millisecond. With these time steps all of the volumes were examined, time slice by time slice.

CHAPTER 5

RESULTS

This chapter will present the results, which are exclusively figures from programming, processing and interpreting with software. This chapter will be followed by an analysis and discussion chapter and last a conclusion chapter.

5.1 Sensitivity investigation

Section 4.1.1 is describing the Matlab model generating results for the sensitivity investigation. The investigation is based on a ray tracing model with variations of target layer thickness, dominant frequency of source wavelet and velocity of target layer. The layered model generated are presented in figure 5.1. The different colours are representing velocities starting from top with the propagation velocity in water. For a text description of how the the layers were modelled see section 4.1.1 or see figure 5.1 for the resulting model. At the interface between two layers with different velocities, wavelets were generated creating traces. In figure 5.2 to 5.13 the wavelets are present interfaces between layers, where the red arrow indicated the target layer.

Figure 5.2 to 5.13 present the main results from the sensitivity investigation. The simulator generated target layers for 2, 4, 6, 8 and 10 meters, which were run with all possible combinations of dominant frequency of source wavelet (30, 50, 70, 90 Hz) and wave propagation velocity for target layer (1600, 1800, 1900, 2500 m/s). Not all the results generated from the combinations are presented, only the figures of minimum detectable layers. The results generated for target

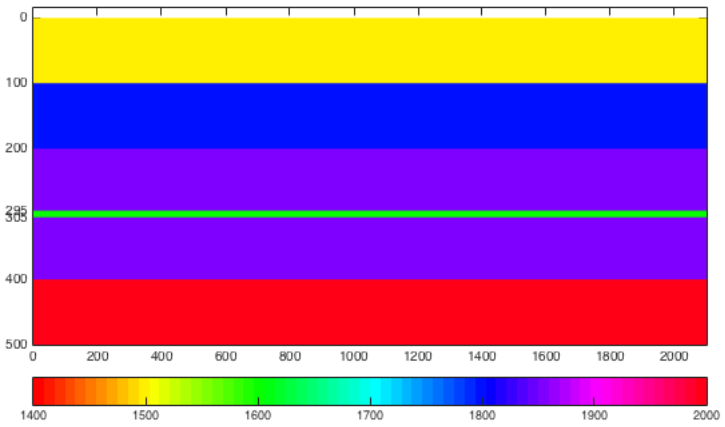

Figure 5.1: Layered geology model generated in Matlab. At the interface between two velocities reflection coefficients were calculated for the ray tracing and generating wavelets. The last layer has a velocity of 2000 m/s.

layers 4, 6 and 8 meters are presented for the corresponding frequencies that they can be detected. For the thickest target layer, 10 meters, the lowest dominant frequency was consistently enough for mapping, this made it unnecessary to include while this target layer thickness was not constrained by any pf the investigated parameters. Opposite the target layer of 2 meters could not be detected for any velocity or frequency combination. More synthetic results were produced and are presented in appendix C in the web version.

Each figure, 5.2 to 5.13, are marked with a red arrow indicating the target layer, which is the target for analysis. The X-axis is showing a length scale in meter where each wavelet is positioned for a common-mid-point [1] (CMP). A CMP is the reflecting point for a seismic ray, for this case with flat reflectors the CMP is midway between the source and receiver along the X-axis. The Y-axis is representing the vertical two-way-time [2] for each interface.

[1] See glossary in appendix A.
[2] See glossary in appendix A.

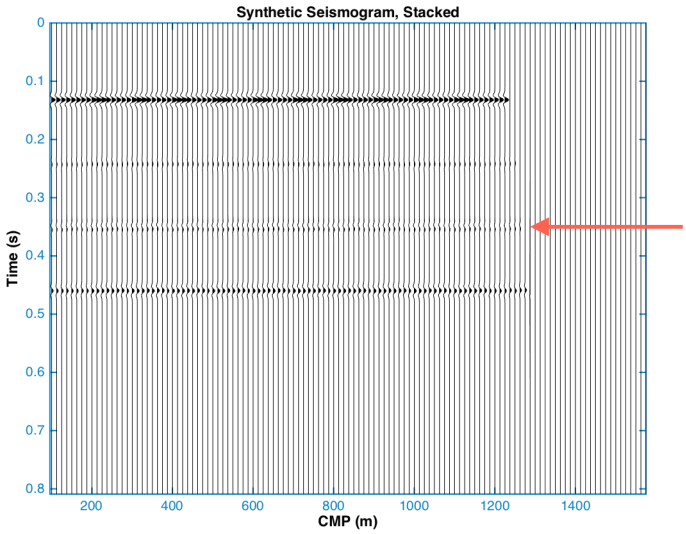

Figure 5.2: Target layer: 4 m, 1800 m/s. Dominant frequency of source wavelet 50 Hz. The red arrow is indicating the target layer.

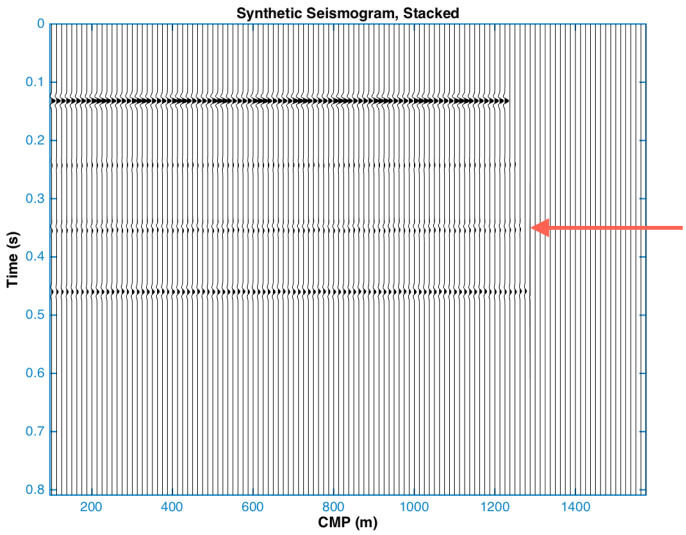

Figure 5.3: Target layer: 6 m, 1800 m/s. Dominant frequency of source wavelet 50 Hz. The red arrow is indicating the target layer.

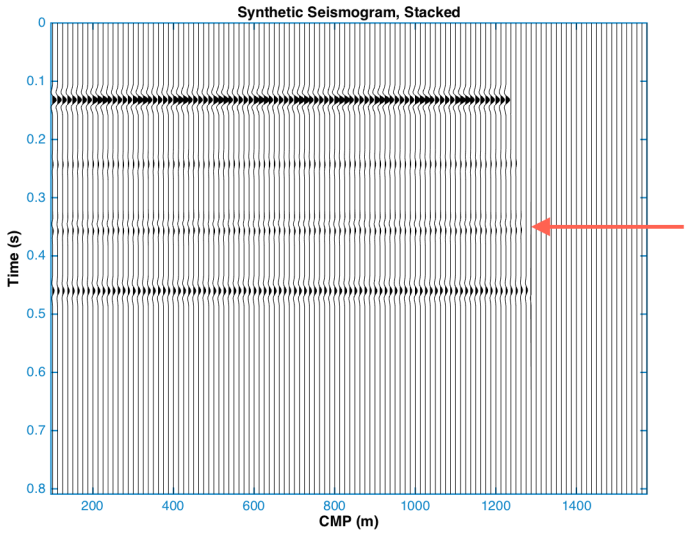

Figure 5.4: Target layer: 8 m, 1800 m/s. Dominant frequency of source wavelet 30 Hz. The red arrow is indicating the target layer.

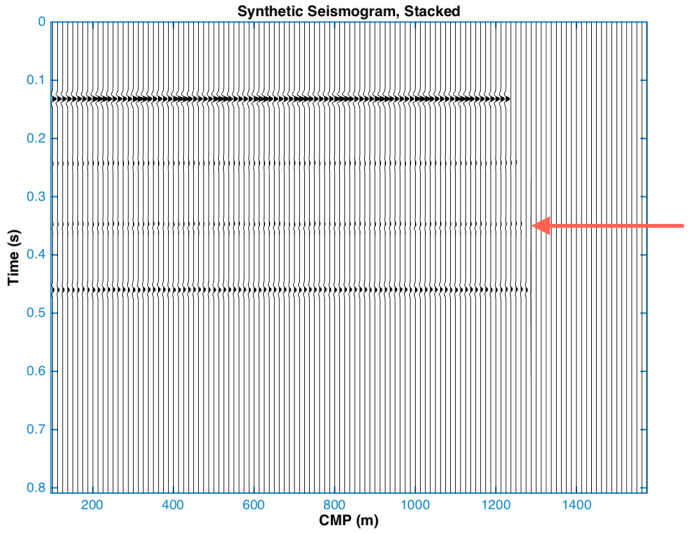

Figure 5.5: Target layer: 4 m, 1900 m/s. Dominant frequency of source wavelet 50 Hz. The red arrow is indicating the target layer.

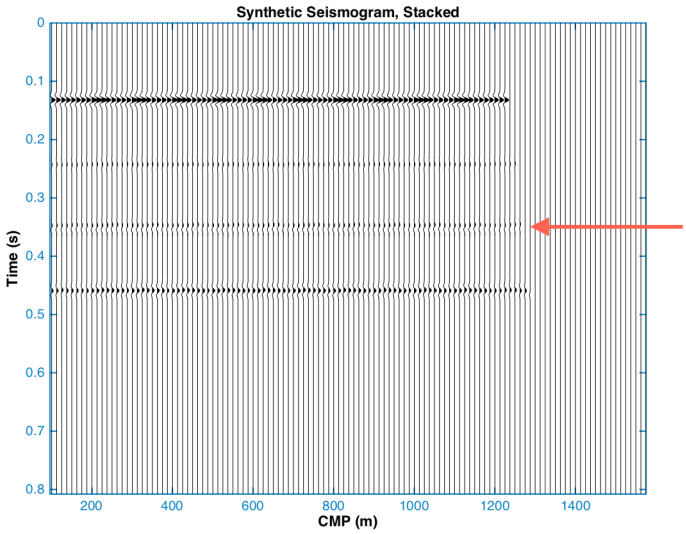

Figure 5.6: Target layer: 6 m, 1900 m/s. Dominant frequency of source wavelet 50 Hz. The red arrow is indicating the target layer.

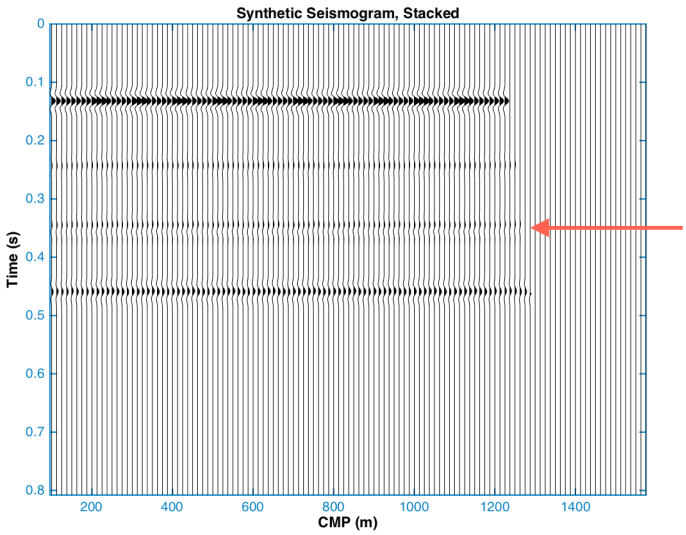

Figure 5.7: Target layer: 8 m, 1900 m/s. Dominant frequency of source wavelet 30 Hz. The red arrow is indicating the target layer.

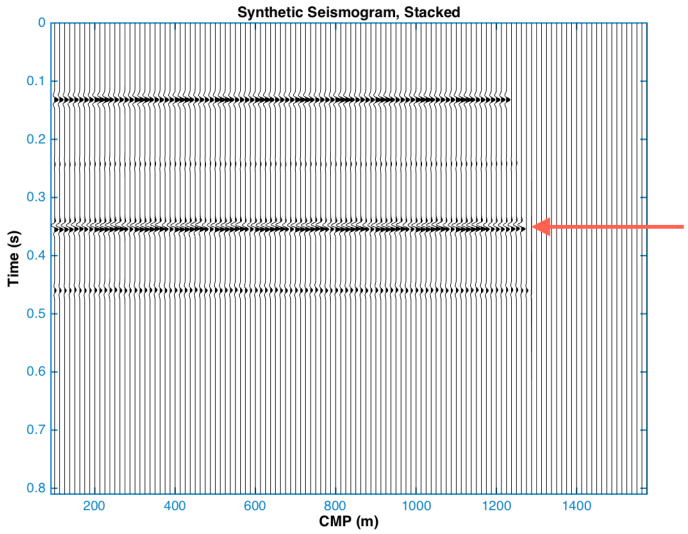

Figure 5.8: Target layer: 8 m, 1600 m/s. Dominant frequency of source wavelet 50 Hz. The red arrow is indicating the target layer.

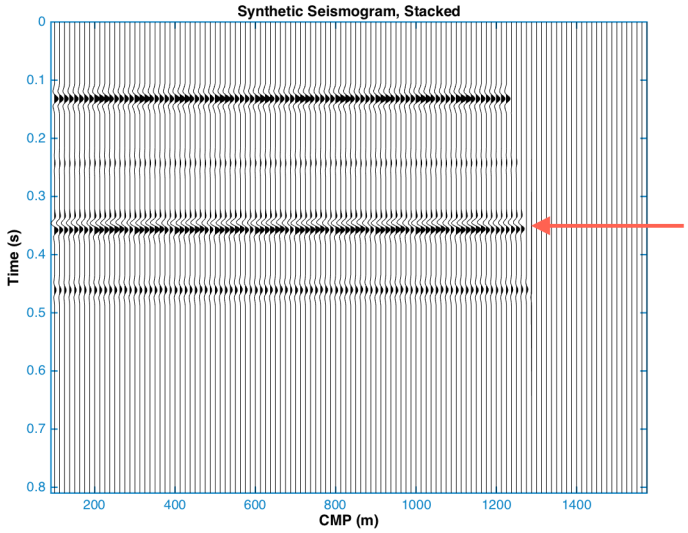

Figure 5.9: Target layer: 8 m, 1600 m/s. Dominant frequency of source wavelet 50 Hz. The red arrow is indicating the target layer.

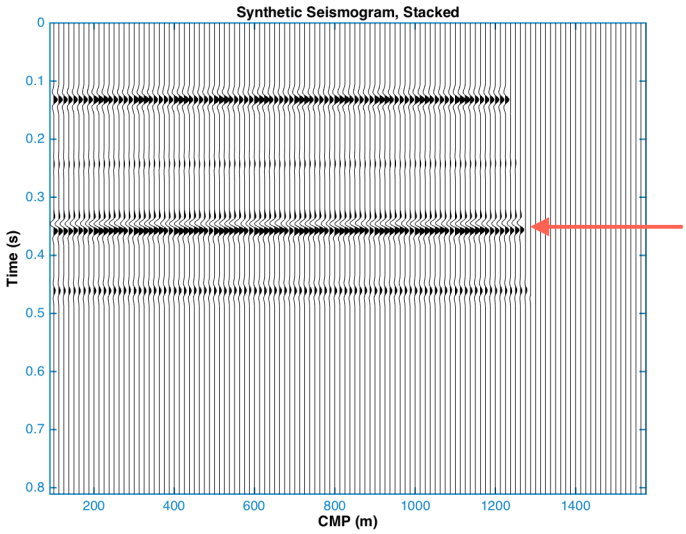

Figure 5.10: Target layer: 8 m, 1600 m/s. Dominant frequency of source wavelet 50 Hz. The red arrow is indicating the target layer.

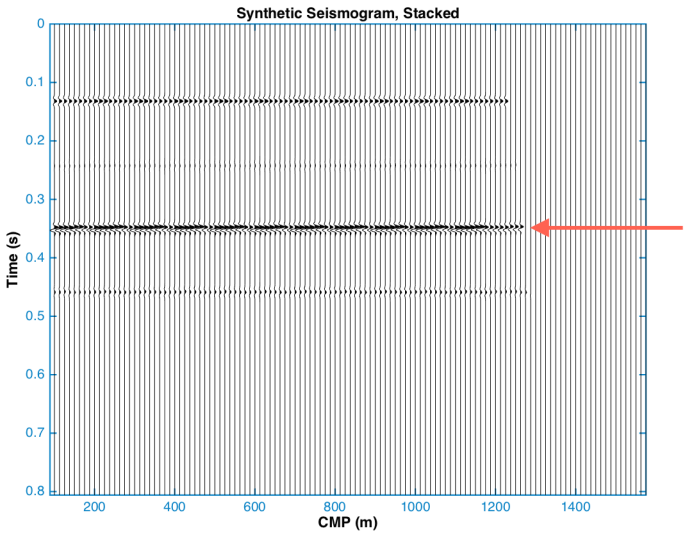

Figure 5.11: Target layer: 4 m, 2500 m/s. Dominant frequency of source wavelet 70 Hz. The red arrow is indicating the target layer.

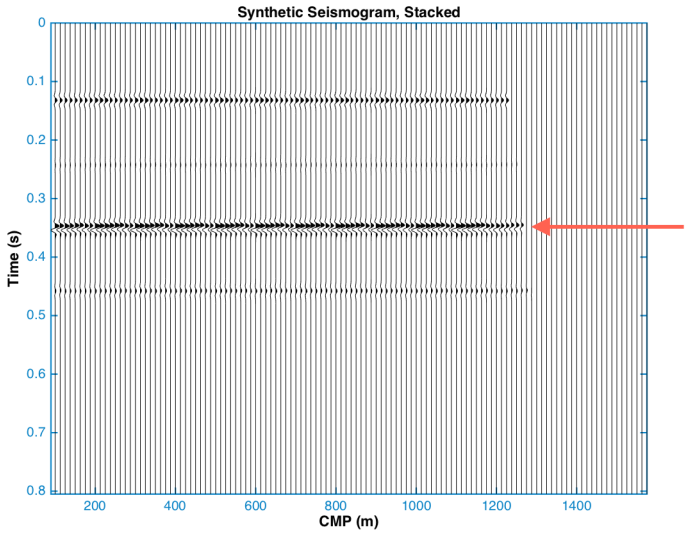

Figure 5.12: Target layer: 6 m, 2500 m/s. Dominant frequency of source wavelet 50 Hz. The red arrow is indicating the target layer.

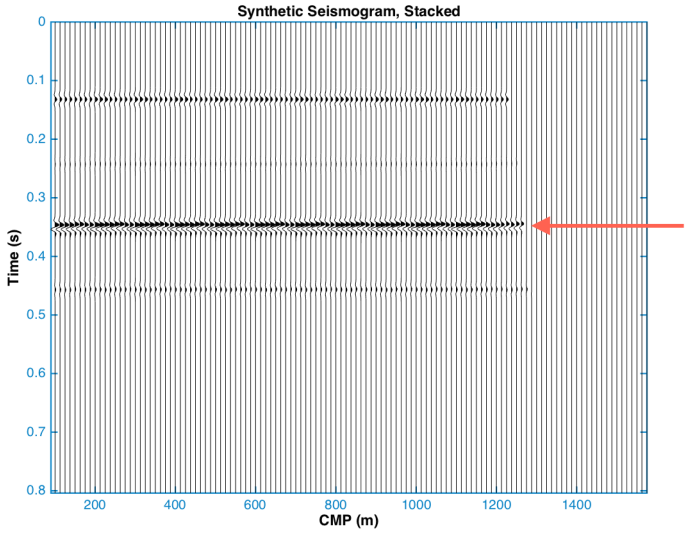

Figure 5.13: Target layer: 8 m, 2500 m/s. Dominant frequency of source wavelet 50 Hz. The red arrow is indicating the target layer.

5.2 Conventional processing, high definition processing and dedicated high resolution

Results from the processing are presented under subsection 5.2.1. The frequency content in an arbitrary line from the high definition processed 3D data is investigated. First in subsection 5.2.2 the three seismic volumes are presented: conventionally processed 3D, high definition processed 3D and dedicated high resolution 2D. From the later two volumes horizons [3] are presented with coherent attributes. Secondly in subsection 5.2.2 time slices [4] from 160, 210, 280, 500 and 1240 milliseconds two way time are presented. A time slice is an extracted figure of an exact time over an area, which has nothing to do with occurrences like layers. The comparable volumes are presented next to each other for each time slice. To illustrate certain differences between the surveys and processing sequences some figures are presented a second time. At last in subsection 5.2.2 selected time slices are scaled up and compared.

Important to have in mind when comparing is that the acquisition parameters are different. That is also what is the purpose of this comparison study; to investigate the dissimilarities of the high definition processed imaging and the dedicated high resolution 2D survey imaging. These two acquisitions differ in the set up, for source as well as receiver parameters. The source, consequently the amplitude and frequency spectra, the receiver set up, which impacted the azimuth and sampling interval, were important differences between the two acquisitions. What impact these differences have and the dissimilarities of the acquisitions is explained in section 2.8, 2.3.2, 2.4.3 and 3.3.

5.2.1 Frequency content investigation

One arbitrary inline [5] from the narrow azimuth 3D streamer acquisition that is processed for a shallow high definition purpose is investigated here. Bandpass filtering and muting are performed in the software OpenCPS. This section will present the results from the frequency investigation. Figure 5.14 shows the result of just stacking [6] without any mute [7] or bandpass filtering [8], then mute are applied from 5.15. Figure 5.16 to 5.19 shows the results of the frequency filtration.

[3] See glossary in appendix A.
[4] See glossary in appendix A.
[5] See glossary in appendix A.
[6] See glossary in appendix A or section 2.4.4.
[7] See glossary in appendix A or section 2.4.4.
[8] See section 2.4.3.

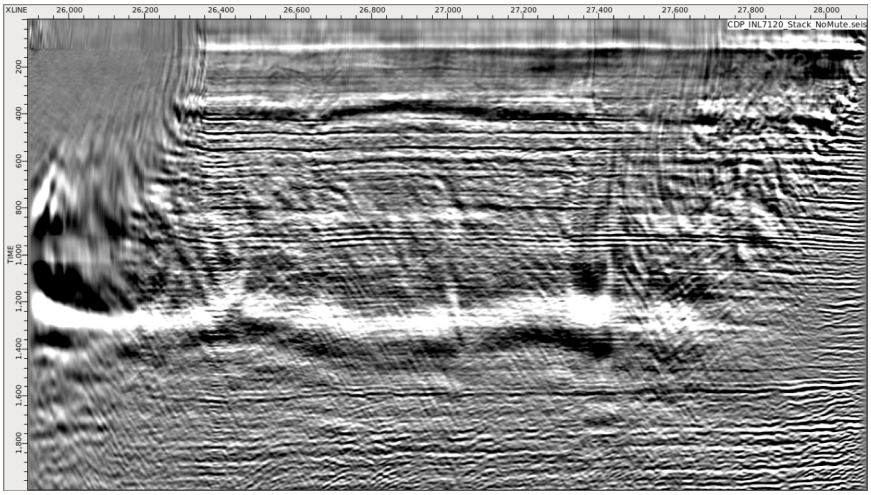

Figure 5.14: The inline acquired with narrow azimuth 3D streamers and high definition processed is here stacked without muting. X-axis is the CMP numbering with equal spacing. Y-axis is the two-way-time, expressed in seconds.

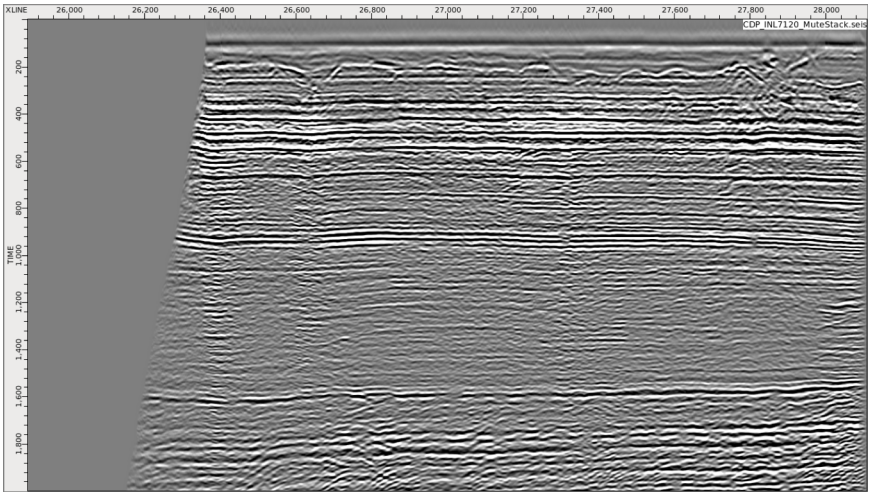

Figure 5.15: The inline acquired with narrow azimuth 3D streamers and high definition processed is here muted and stacked. X-axis is the CMP numbering with equal spacing. Y-axis is the two-way-time expressed in seconds.

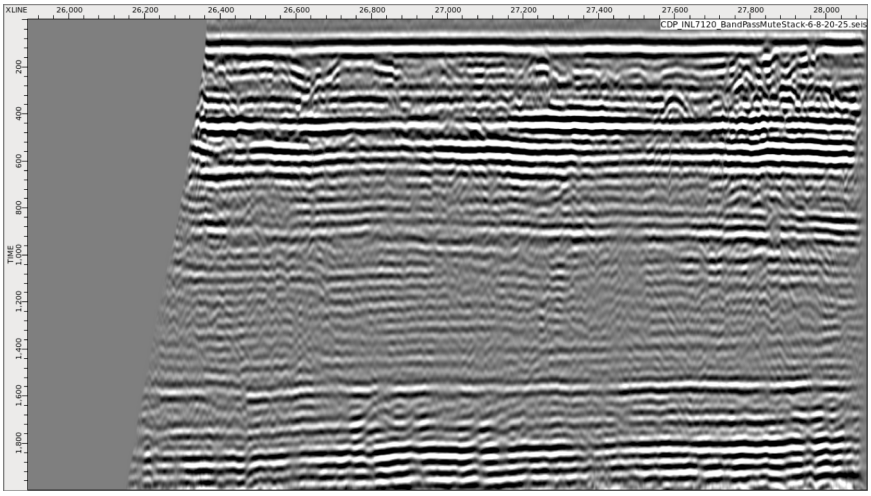

Figure 5.16: The inline acquired with narrow azimuth 3D streamers and high definition processed is here frequency filtered and passed for 6-25 Hz. It is also muted and stacked. X-axis is the CMP numbering with equal spacing. Y-axis is the two-way-time expressed in seconds.

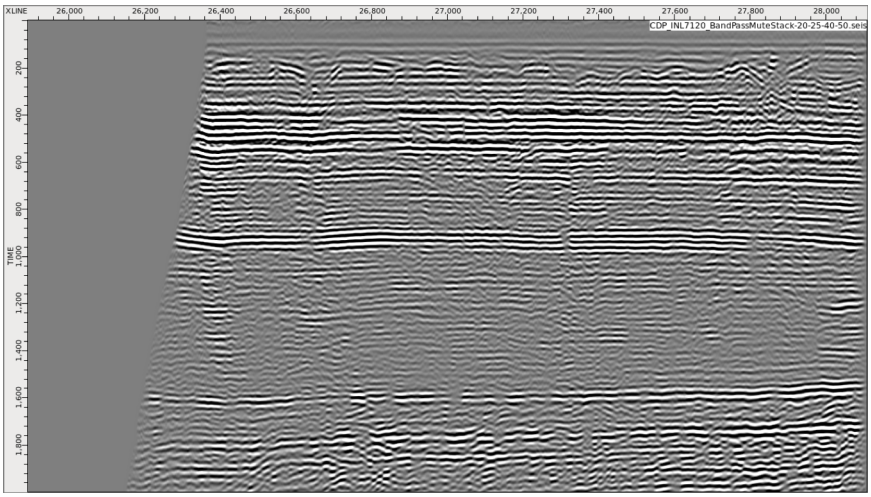

Figure 5.17: The inline acquired with narrow azimuth 3D streamers and high definition processed is here frequency filtered and passed for 20-50 Hz. It is also muted and stacked. X-axis is the CMP numbering with equal spacing. Y-axis is the two-way-time expressed in seconds.

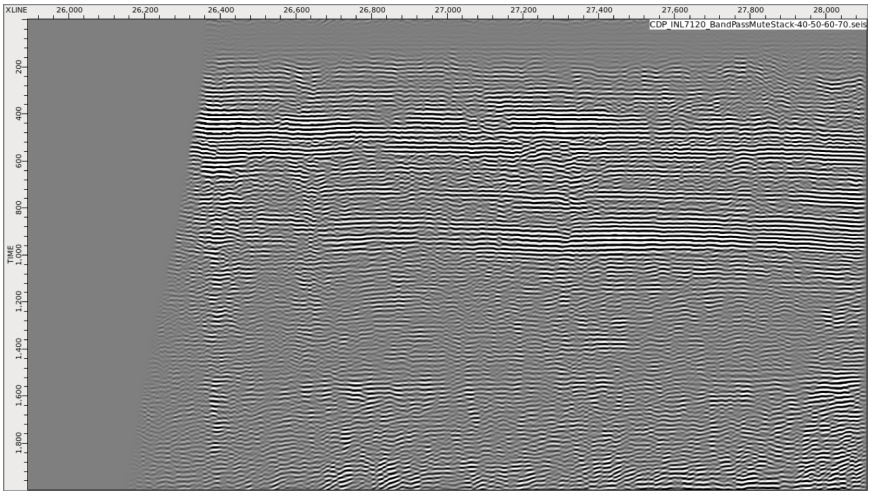

Figure 5.18: The inline acquired with narrow azimuth 3D streamers and high definition processed is here frequency filtered and passed for 40-70 Hz. It is also muted and stacked. X-axis is the CMP numbering with equal spacing. Y-axis is the two-way-time expressed in seconds.

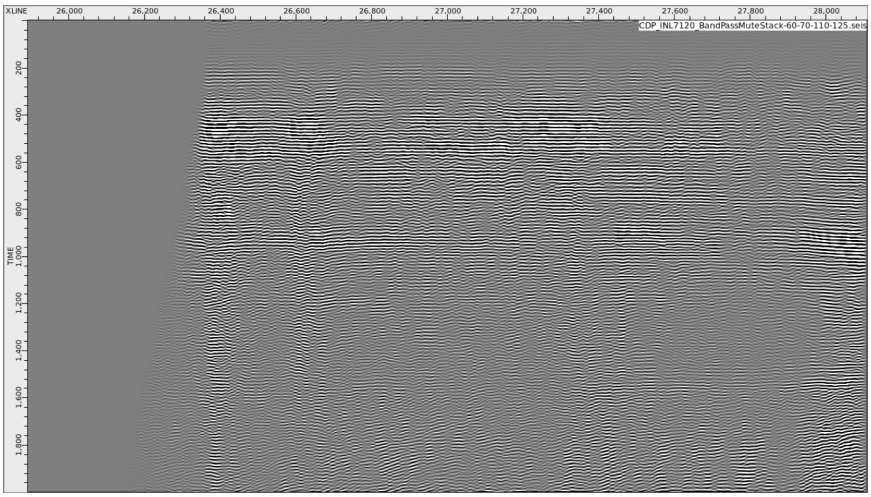

Figure 5.19: The inline acquired with narrow azimuth 3D streamers and high definition processed is here frequency filtered and passed for 60-125 Hz. It is also muted and stacked. X-axis is the CMP numbering with equal spacing. Y-axis is the two-way-time expressed in seconds.

5.2.2 Seismic volume interpreting

Here below are the three seismic volumes, four horizons [9] and five time slices [10] to be compared. The seismic volumes represents the work material from where the horizons where picked as well as the time slices extracted from and give the reader a hint of the bigger picture. How the horizons were picked and the time slices examined are described in section 4.2.2.

Seismic volumes

First the three seismic volumes are presented: conventionally processed 3D, high definition processed 3D and dedicated high resolution 2D. No depth times are presented with regards to constraints from Maersk Oil.

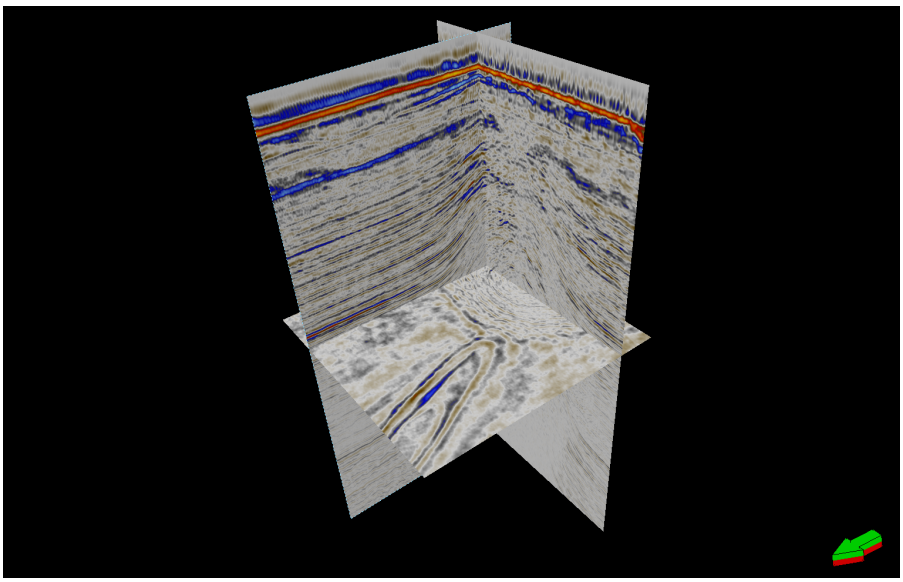

Figure 5.20: Conventionally processed imaging of the narrow azimuth 3D streamer shallow water acquired data set. Centred in the corner of the two vertical panes something like a "hill" is emerging, which probably is a fractured salt dome.

[9] See glossary in appendix A.
[10] See glossary in appendix A.

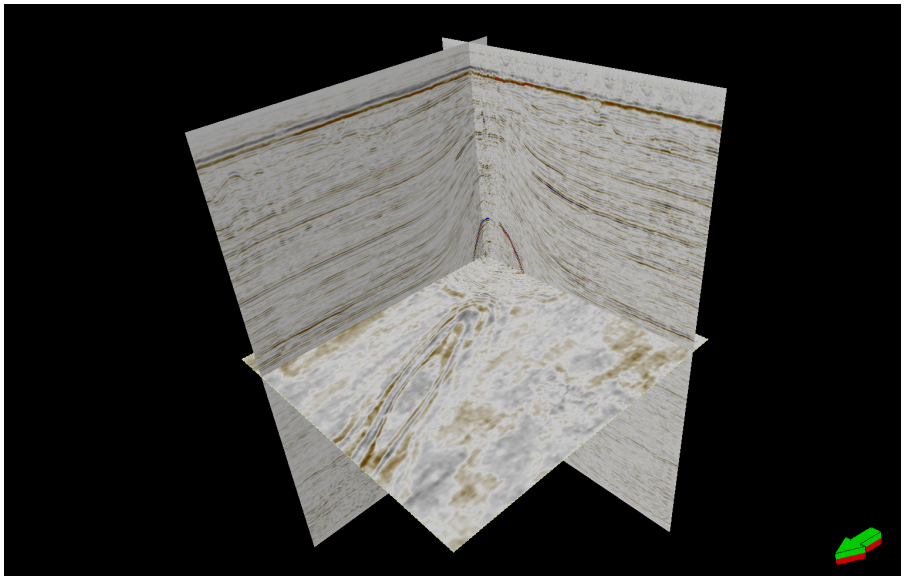

Figure 5.21: High definition reprocessed imaging of the narrow azimuth 3D streamer shallow water acquired data set. Centred in the corner of the two vertical panes something like a "hill" is emerging, which probably is a fractured salt dome.

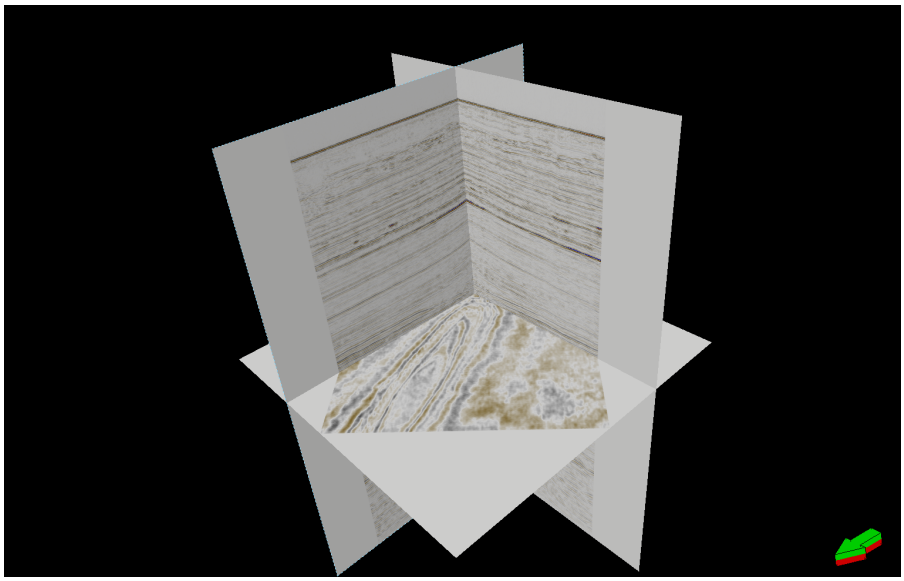

Figure 5.22: Processed imaging of the dedicated high resolution 2D acquisition.

Horizons and their attributes

First horizons [11] where picked at the seabed for the two volumes from high definition 3D processed and dedicated high resolution 2D data. The second horizon where picked at an arbitrary depth. From the horizons three attributes were extracted: two-way-time [12], amplitude and dominant frequency. As mentioned in the beginning of this section it is the comparison that is important. The colour scales are more or less useless while the two different acquisitions will generate different scales for the attributes. Important to compare is how the attributes varies over the area, i.e. how the colours changes. Comparable figures are the ones showing the same attribute at the same horizon level from the high definition imaging and the dedicated high resolution 2D imaging. They are coupled at one page and viewed upon from the same direction, which is indicated by the green arrow in the lower right corner.

[11] See glossary in appendix A.
[12] See glossary in appendix A.

The comparable figures are from here on picked at the seabed, and attributes are extracted from that picked horizon.

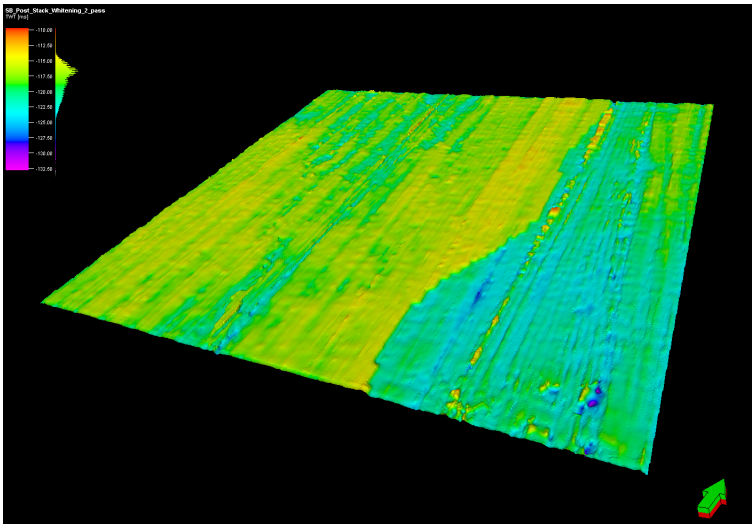

Figure 5.23: Seabed surface picked from the high definition 3D processed volume. The seabed is coloured with variations in two-way-time.

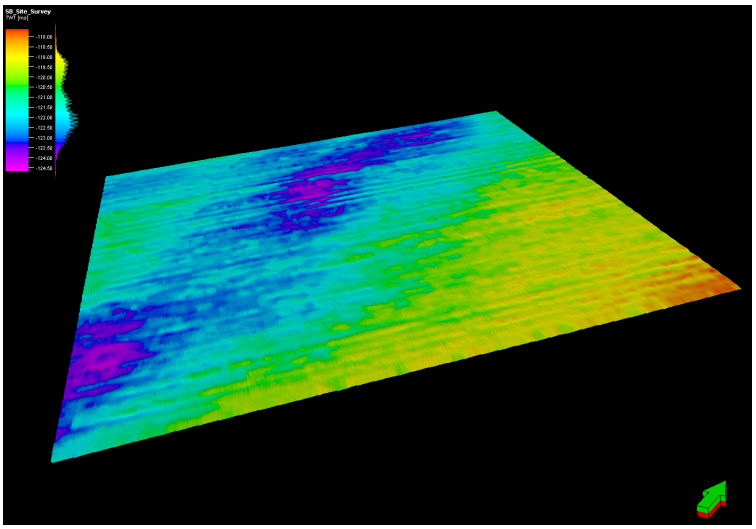

Figure 5.24: Seabed surface picked from the dedicated high resolution 2D survey volume. The seabed is coloured with variations in two-way-time.

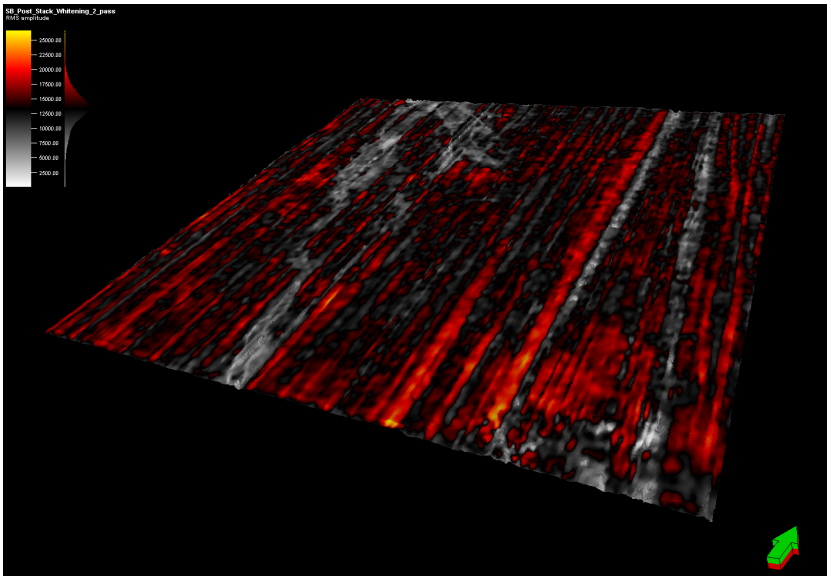

Figure 5.25: Extracted amplitude attribute at the seabed horizon from the high definition 3D processed volume, variations in colour is due to different amplitude in reflected traces.

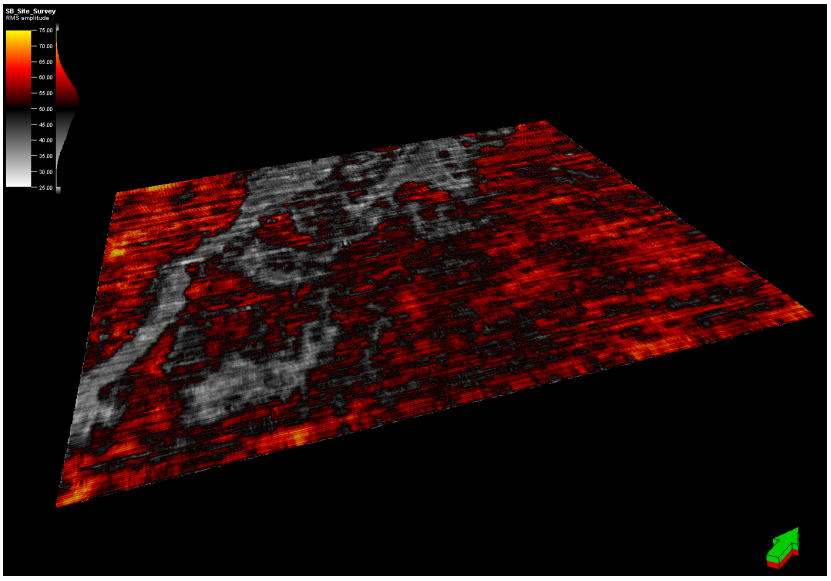

Figure 5.26: Extracted amplitude attribute at the seabed horizon from the dedicated high resolution 2D survey volume, variations in colour is due to different amplitude in reflected traces.

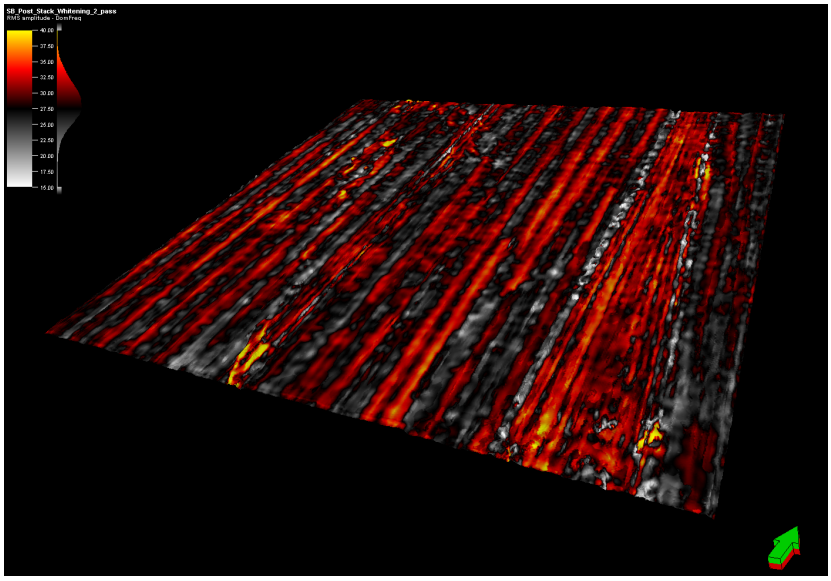

Figure 5.27: Extracted dominant frequency attribute at the seabed horizon from the high definition 3D processed volume, variations in colour is due to different frequency for reflected traces.

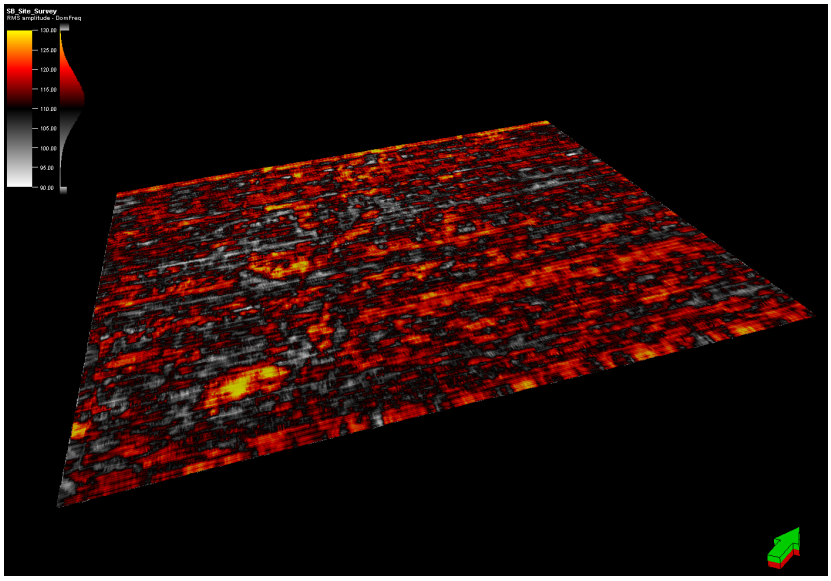

Figure 5.28: Extracted dominant frequency attribute at the seabed horizon from the dedicated high resolution 2D survey volume, variations in colour is due to different frequency for reflected traces.

From here on the comparable figures are picked at an arbitrary depth, and attributes are extracted from that picked horizon [13]. With the purpose of extracting attributes at two horizons at the same level and compare. Does the two different acquisitions indicate the same features?

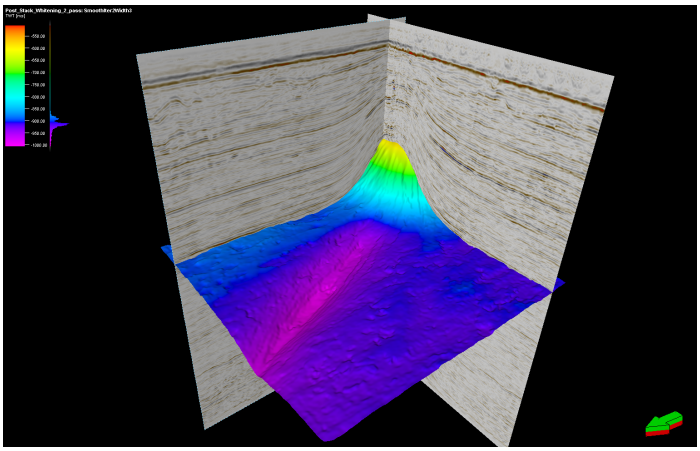

Figure 5.29: Horizon picked from what is interpreted as a layer for the high definition processed 3D volume. The horizon is coloured with variations in two-way-time. Centred in the corner of the two vertical panes, something like a "hill" is emerging, which probably is a fractured salt dome. The dome is marked from the top with yellow, then green switching to turquoise.

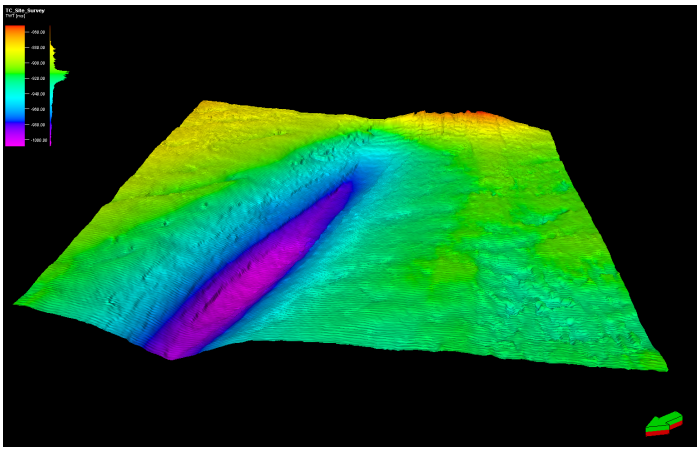

Figure 5.30: Horizon picked from dedicated high resolution 2D survey volume and is interpreted as a layer at the same level as illustrated in figure 5.29. The horizon is coloured with variations in two-way-time.

[13] See glossary in appendix A.

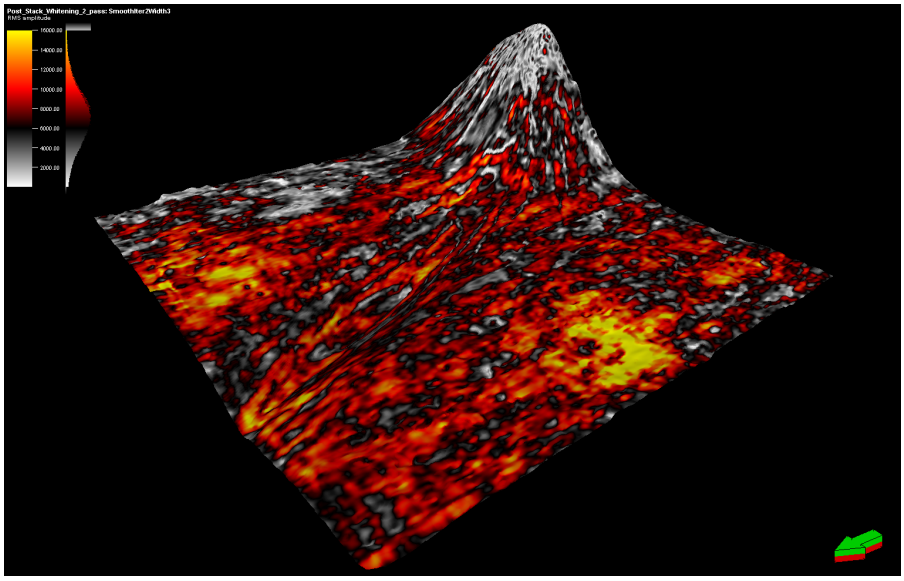

Figure 5.31: Extracted amplitude attribute at horizon in 5.29 from high definition processed 3D volume, variations in colour is due to different amplitude in reflected traces..

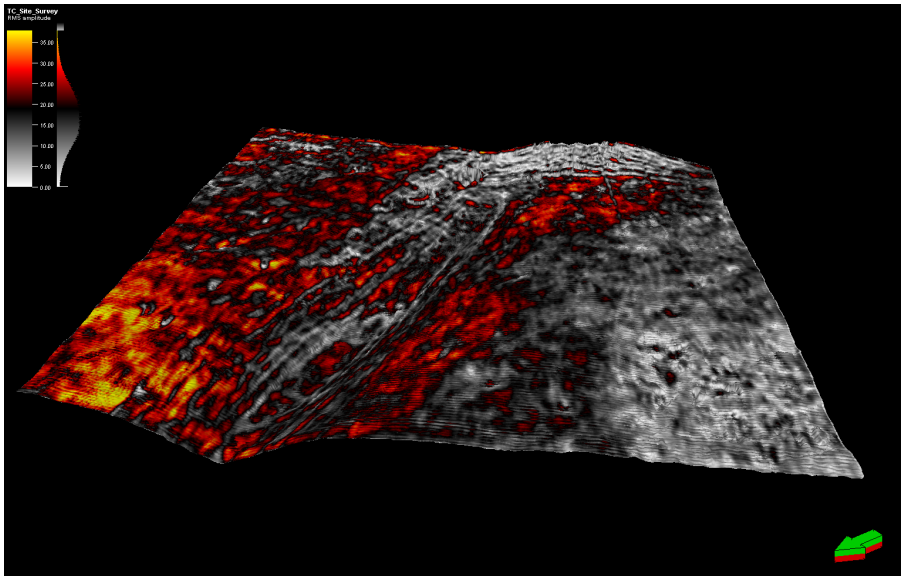

Figure 5.32: Extracted amplitude attribute at horizon in 5.30 from dedicated high resolution 2D survey volume, variations in colour is due to different amplitude in reflected traces..

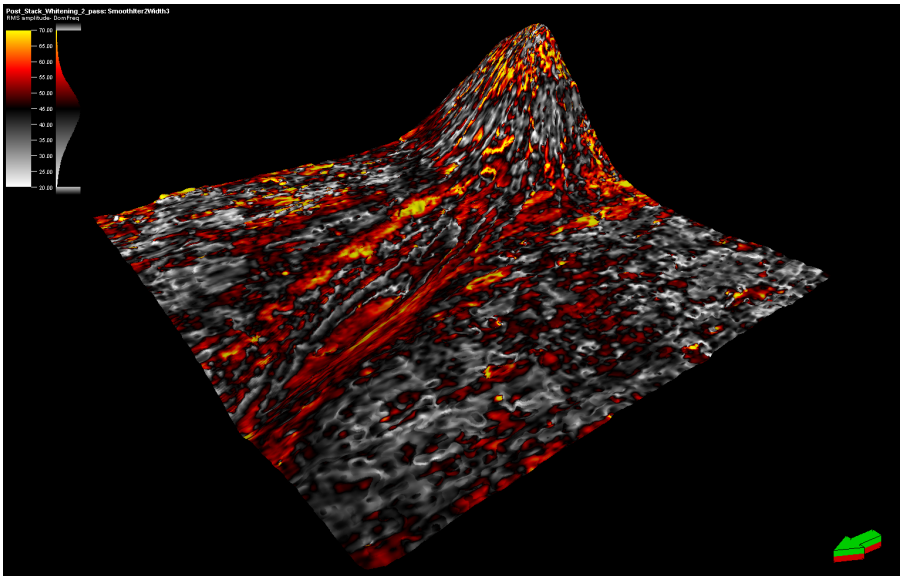

Figure 5.33: Extracted dominant frequency attribute at horizon in 5.29 from high definition processed 3D volume, variations in colour is due to different frequency for reflected traces.

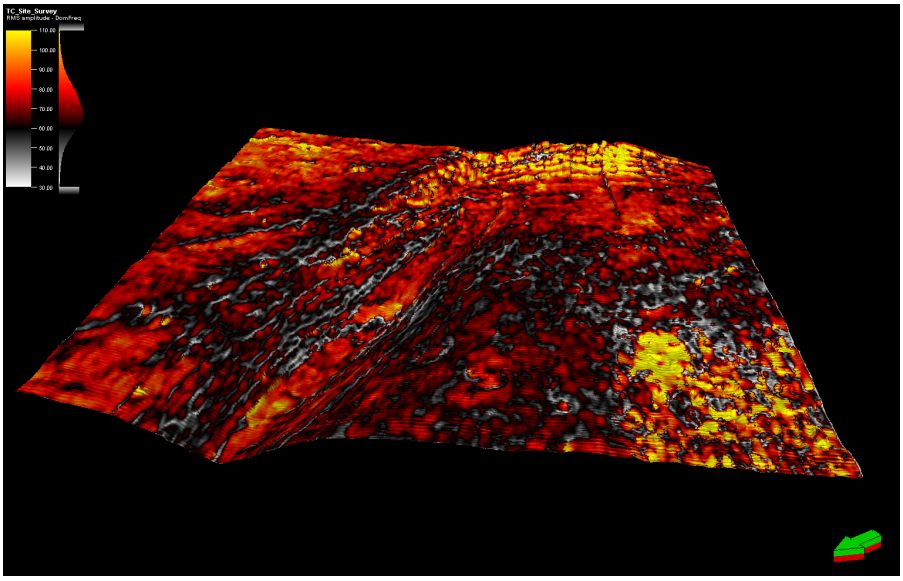

Figure 5.34: Extracted dominant frequency attribute at horizon 5.30 from dedicated high resolution 2D survey volume, variations in colour is due to different frequency for reflected traces.

Time slices

From this point time slices [14] from the three different volumes are presented next to each other. The figures 5.35 to 5.39 are presenting the conventionally processed 3D data in subfigure (a), high definition 3D processed image in (b) and dedicated high resolution 2D image in (c). Later larger figures for some of the time slices interesting for closer comparison are presented, only between the high definition processed image and dedicated high resolution 2D image. The colour scale ranges between black and white, where black is traces of high amplitude and vice versa. For how the examination of the time slices were made are described in section 4.2.2.

For the images below, subfigure (b) is the one to be compared to both (a) and (c). When comparing these time slice images, as when comparing the horizons [15], one should look for similarities as well as features that do not conform between (b) and (c). For the the case of comparing (a) to (b) one should look if (b) is any clearer than (a) and if (b) makes more sense.

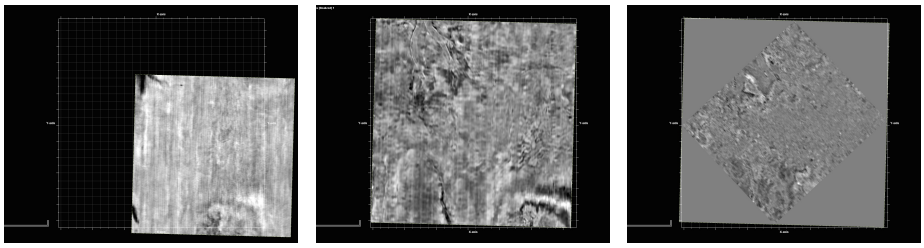

(a) (b) (c)

Figure 5.35: Time slices at 160 milliseconds. The time slices are extracted from the three different seismic volumes: (a) conventionally processed deep seismic imaging, (b) high definition processed imaging and (c) dedicated high resolution 2D survey imaging.

The next three panes in figure 5.39 are actually below what here is referred to as shallow subsurface but can still help understanding the concept of these three different volumes. Importantly how subfigure (c) loses resolution relative to subfigure (a) and (b). This level is below the target of the dedicated high resolution 2D acquisition, and can be acknowledged by comparing the resolution of (a) and (c) in figure 5.39. This time slice [16], at 1240 milliseconds, is not only below the target of the 2D survey but also on the boarder of the target for the conventionally acquired 3D survey.

[14] See glossary in appendix A.
[15] See glossary in appendix A.
[16] See glossary in appendix A.

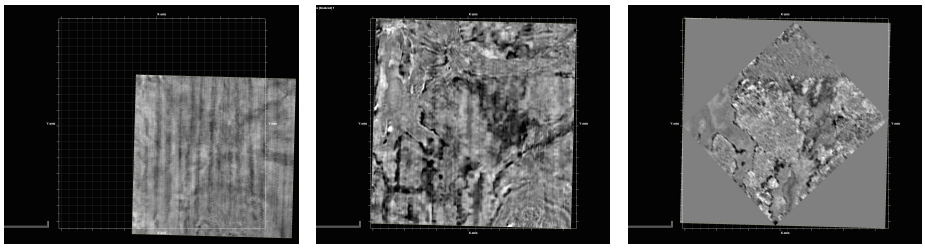

(a) (b) (c)

Figure 5.36: Time slices at 210 milliseconds. The time slices are extracted from the three different seismic volumes: (a) conventionally processed deep seismic imaging, (b) high definition processed imaging and (c) dedicated high resolution 2D survey imaging.

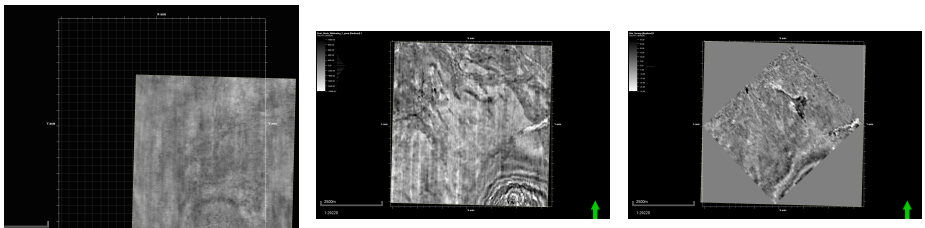

(a) (b) (c)

Figure 5.37: Time slices at 280 milliseconds. The time slices are extracted from the three different seismic volumes: (a) conventionally processed deep seismic imaging, (b) high definition processed imaging and (c) dedicated high resolution 2D survey imaging.

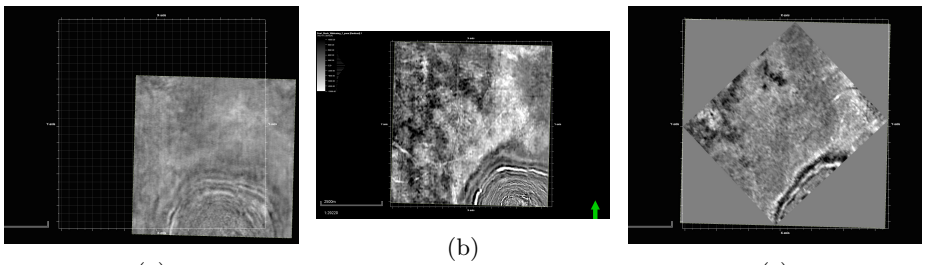

(a) (b) (c)

Figure 5.38: Time slices at 500 milliseconds. The time slices are extracted from the three different seismic volumes: (a) conventionally processed deep seismic imaging, (b) high definition processed imaging and (c) dedicated high resolution 2D survey imaging.

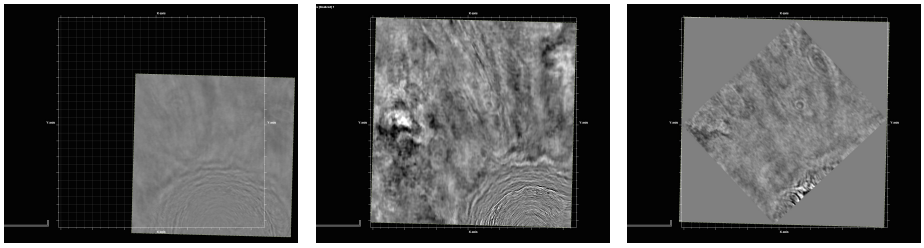

(a) (b) (c)

Figure 5.39: Time slices at 1240 milliseconds. The time slices are extracted from the three different seismic volumes: (a) conventionally processed deep seismic imaging, (b) high definition processed imaging and (c) dedicated high resolution 2D survey imaging.

Selected time slice comparison

The subfigures (a) and (b) in figure 5.37 and 5.38 is of such interest that they are scaled up in figure 5.40 to 5.43. These time slices [17] holds interpretational differences in imaging of the same time slices, which are marked in the figures. Under certain interest in these figures are two black spots and one line, which are marked with red rings and arrows. One figure is presented per sheet and should be compared in pairs. First the high definition 3D processed image and thereafter, on the next page, the image from the dedicated high resolution 2D data.

Figure 5.40 show the time slice of 280 milliseconds for the high definition 3D processed image, where black spots can be seen. These black sports are for example what an interpreter are looking for, they could indicate a geohazard. For how the examination of the time slices were made are described in section 4.2.2.

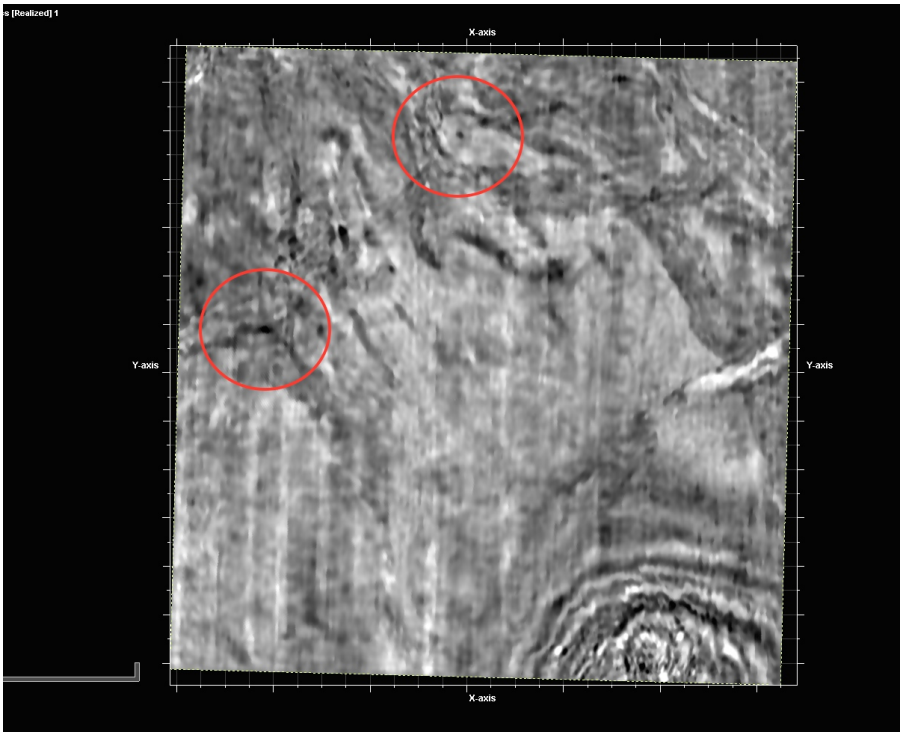

Figure 5.40: High definition processed 3D image of time slice 280 milliseconds. At the centre of the circles shows what can not be seen in the comparable imaging of the dedicated high resolution 2D survey.

[17] See glossary in appendix A.

Figure 5.41 show the corresponding time slice for the dedicated high resolution 2D survey image at 280 milliseconds. The same areas as in the high definition 3D image are marked with red rings, where no strong anomalies as black or white colour stand out.

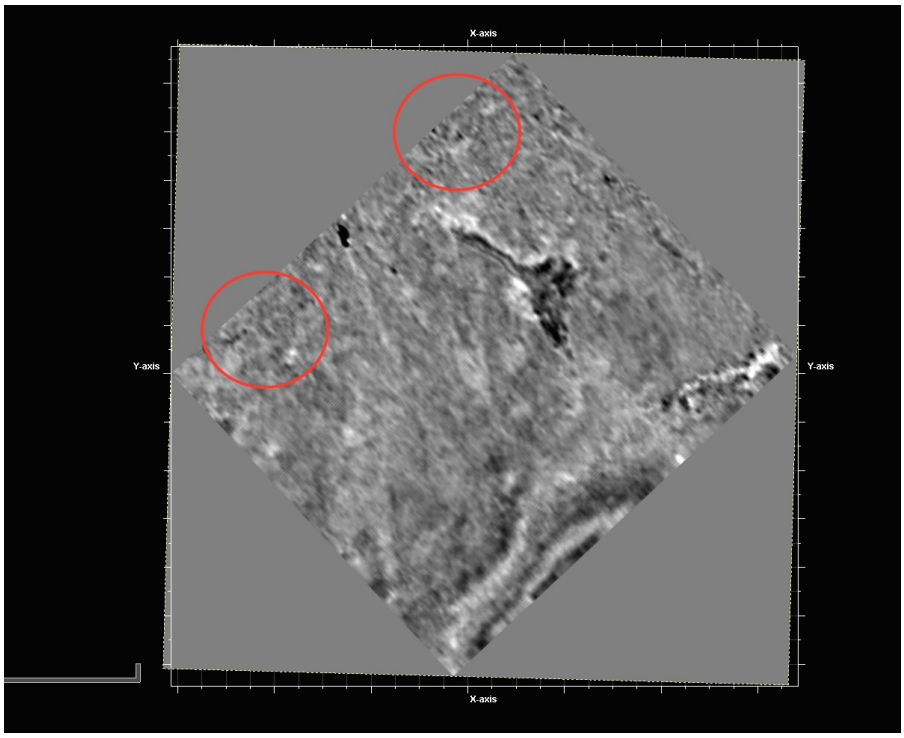

Figure 5.41: Image from the dedicated high resolution 2D survey of time slice 280 milliseconds. The red marked circles are placed at the exact same position as for the high definition processed 3D image 280 milliseconds time slice.

Figure 5.42 show an interesting feature, namely the line stretching northeast indicated by red arrows. The inline [18] for the survey of this image, 5.42, is 45 degrees towards the line, hence the line is properly mapped. The most interesting is not the fact this line show in this image but that it does not show in the dedicated high resolution 2D survey image.

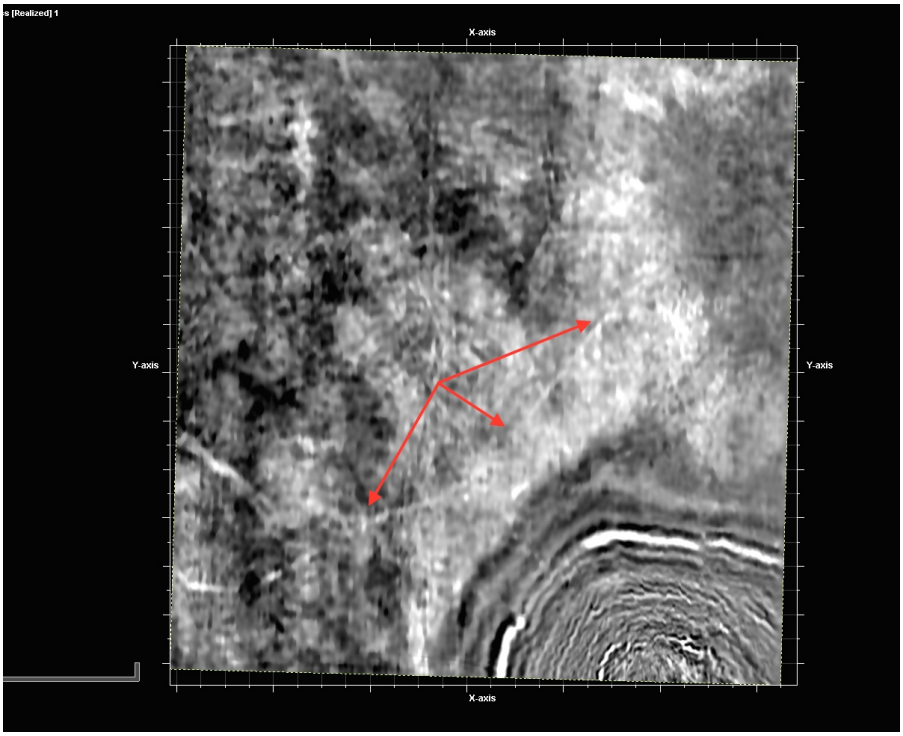

Figure 5.42: High definition 3D processed image of time slice 500 milliseconds. A line are marked with red arrows.

[18] See glossary in appendix A.

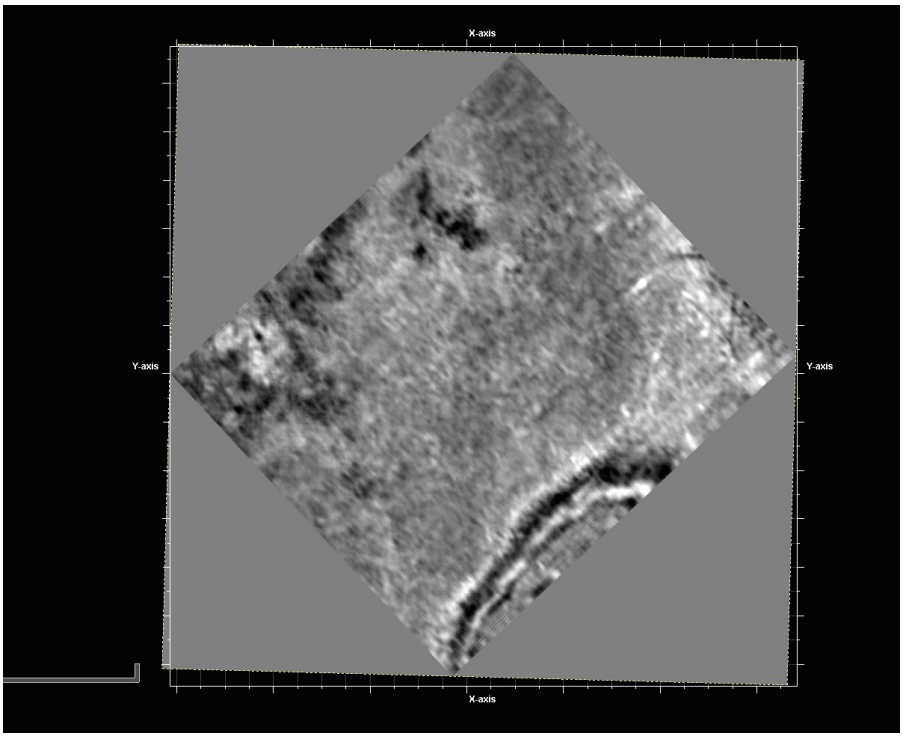

Figure 5.43: Image from the dedicated high resolution 2D survey of time slice 500 milliseconds. This figure is not marked.

Figure 5.43 has no highlights due to that the targeted line in the high definition 3D image can not be seen in the dedicated high resolution 2D survey image.

All the salient spots and lines in the different time slices [19] that can be seen in the high definition processed image but not in the 2D acquisition image have been investigated at time slices deeper and above. Not deeper nor above can the spots or lines be seen as clear as for the high definition processed 3D image.

Different processing sequences are needed for the 3D and 2D data sets. Time slices might therefore not overlap exactly in depth time. This is what initiated the extra investigation above and under what is presented here and can be found in appendix.

[19] See glossary in appendix A.

CHAPTER 6

ANALYSIS AND DISCUSSION

This report aims at investigating the outcome of an alternative processing sequence for extending the resolution of conventional processing for deep seismic 3D acquired data at shallow water depths to image shallow subsurface targets. Firstly an sensitivity investigation was made by a model generating synthetic data, as basis for investigating the degree of resolution for the high definition processed 3D image. Secondly one arbitrary inline [1] of the high definition 3D processed data was investigated from an bandwidth perspective to study the frequency content, important for resolution. Thirdly and last the dedicated high resolution 2D data, high definition processed 3D data and conventionally processed 3D data was displayed as a volumes. Horizons [2] were picked from the first two volumes and attributes were extracted from these horizons.

The purpose of the sensitivity investigation was to map weather a thin layer would stand out enough to be detectable. Two attributes were seen important for a minimum detectable layer: amplitude and frequency. Amplitude for the layer to stand out from possible noise, which was not generated in the synthetic model. Frequency for if how close the wavelets could be without too severe overlapping, and therefore not be distinguished. While the synthetic model was generating an amplitude only represented by coefficients, explained in section 2.2.2, the investigation has focused on the separability, i.e. mapping. Consequently the amplitudes were not modelled realistically and therefore not analysed. Other aspects of real acquisitions have not been taken in account and modelled; e.g. like noise, attenuation of seismic energy with depth or multiples.

[1] See glossary in appendix A.
[2] See glossary in appendix A.

Nevertheless the question to be asked is when does the overlapping become a problem? The seismic modelling results were visually analysed. The estimated threshold for where the overlapping is too severe are presented in figures 5.2 to 5.13, and in combination with the different parameters generating each figure. One should keep in mind that output from the modelling is only based on 4 different dominant frequencies: 30, 50, 70, 90 Hz. Likewise the layer thicknesses investigated are separated by 2 meters as 2, 4, 6 etc. This method does not give a smoothness for the analysis and can therefore not give an exact answer to the posed question above, but indicate probable resolution for the high definition 3D imaging in combination with an frequency investigation. No conclusions about the resolution of the high definition 3D imaging can be drawn from this analysis alone without investigating the frequency content of the acquired data.

If there would be a ratio of the wavelength for layers to be detectable this coarse method makes it hard to say. For the figures to form an estimated threshold for layers to be detectable they are all within the range of $\frac{1}{4}$ and $\frac{1}{16}$ of the dominant wavelength, as described in section 2.3.2. It also breaks down to an Ω between 6 and 10 from equation 2.14. The Ω is on average 7.8 with an standard deviation of 1.2. What frequency content is important to be able to accurately illustrate the shallow subsurface? Depending on wave propagation velocities and layer thicknesses of interest different frequencies are desired. The analysis made here indicate that a frequency range from 30 to 70 Hz is desirable. Hence the frequency content of the shallow reflections is interesting to investigate. How the model simulation is done is described in section 4.1.1.

With tools in the software OpenCPS one arbitrary streamer inline of the high definition processed conventional 3D acquired data were investigated. The figures 5.16 to 5.19 illustrates how much data each one of the four frequency bandwidths holds, and they were compared with the full bandwidth vertical figure. This inline were assumed to be representative for the whole high definition 3D processed volume. The figures also show clearly how data with different frequencies are collected from different depths. This analysis, done from the figure output of the high definition data in OpenCPS, shows that reflections holds considerable information within the four frequency bandwidths ranging from 3 to 125 Hz. That frequency range is far wider than the frequency range examined in the synthetic modelling. Hence the frequency investigations of the high definition 3D processed data suggests that the volume should be able to resolve also thin layers in the shallow subsurface. When comparing frequencies with the synthetic modelling output yields that this new processing method should resolve, or at least be able to map, layers between 4 and 6 meters thin throughout this high definition 3D processed data set. That makes the high definition processed 3D image interesting not only to compare with the conventionally 3D image but also with the 2D site survey image.

The figures in subsection "Seismic volumes" in section 5.2.2 are displaying the three comparable volumes. These three volumes are presented with the intention

to partly show the differences in resolution over depth and to give the reader an understanding of the whole volumes. From these volumes horizons [3] were picked at the seabed and at an arbitrary depth, and presented in subsection "Horizons and their attributes" in section 5.2.2. Horizons were only picked from the high definition 3D processed volume and the dedicated high resolution 2D survey volume, not from the conventionally processed 3D volume.

From the horizons the attributes two-way-time [4], root mean square amplitude and dominant frequency are extracted. These attributes are extracted with the purpose of finding similarities in the high definition 3D processed and 2D site survey attributes. Important is to look for similar discontinuities in colouring. While the surveys set-up are different one can expect different subsurface response, hence amplitude and frequency response were different. To start with the sea bed horizon, the two-way-time illustrations show two different seabeds, although a green area can be discerned to the left in the high definition 3D image, figure 5.23, overlapping the blue area in the 2D image, 5.24. For the amplitude imaging of the seabed features come forward in almost the same extent for both of the data sets, indicating areas with low and high amplitudes are nearly identical. The last extracted attribute for the seabed, dominant frequency is hard to interpret. The dominant frequency bandwidth are obviously higher for the site survey but wider for the 3D survey over the area. This is expected. Features indicated by partial areas of higher and lower dominant frequencies are corresponding. Severe acquisition footprints [5] dominate the seabed imaging, worse in the 3D than the 2D. The footprints clear away with depths for the volume acquired by a 3D survey, whilst less footprints at the top in the dedicated high resolution 2D volume maintain almost intact deeper down. Nevertheless it is possible to distinguish formations for all the comparable images of the seabed, and they all indicate matching features.

At an arbitrary depth the matching horizons [6] were picked from the two seismic volumes. The same three attributes were extracted for the deeper horizons as for the seabed horizons. Figure 5.29 show from where in the high definition 3D volume the horizon is picked, the same depth applies to the 2D survey interpretation, in figure 5.30. The two-way-time colouring shows two nearly identical horizons, with big similarities for what can be interpreted as ancient channels and the flat horizon besides. The 2D acquired horizon indicates some kind of start of a dome by red in the upper right corner. With respect to being in the outskirts of the 2D survey the start of the dome is recreated stair-like, probably due to that the single line streamer acquisition transversely going over the hill. In contrast to the stair-like dome, the 3D survey imaging is showing more smoothness. The dome is although difficult to image and interpret due to fracture zones as can be seen in figure 5.20 and 5.21 as well as in figure 5.29.

[3] See glossary in appendix A.
[4] See glossary in appendix A.
[5] See glossary in appendix A.
[6] See glossary in appendix A.

The panes at the two-way-time 160, 210, 280, 500 and 1240 milliseconds are interesting for comparable purposes. They clarify differences in a simple illustrative way. Figure 5.35 show a really shallow image of 160 milliseconds where (a) is severely aliased. For the high definition processed (b) big improvements of dealiasing can be seen from (a) but still severe lines disturbing the image remains, appearances from footprints [7]. However the imaging in (c) is the best one at this depth although there are footprints. A little deeper is the 210 milliseconds time slice [8]. At this depth, in figure 5.36, the high definition processed image in (b) are catching up with the 2D survey image in (c). Formations are starting to appear in (b) as can be seen in (c). For the time slice 280 milliseconds interesting differences start to appear in the high definition processed image. Two dark spots stands out in the high definition processed image that do not or hardly appear in the imaging of the 2D survey. These spots are marked in figure 5.40. In the high definition processed image a brighter almost elliptical area occurring with perspective due to azimuth 3D effect. The time slice gives other areas with 3D effects contributing to the overall understanding of the geology. At the next time slice, 500 milliseconds, another interesting feature reveals. Figure 5.42 shows how a bright line stretching in the northeast direction. This line can not be seen but glimpsed in the northeast end in figure 5.43. Why the line is hard to image by the 2D acquisition is because the 2D acquisition survey lines also are in the northeast direction. This fact that the acquired lines, i.e. from source to receiver, have no azimuth, i.e. angle, towards the scorch mark is what makes it hard to image. Lines like this is important to cover. For this case the high definition processed conventional acquired 3D data was of great help to map the line. Marks like the spots in time slice 280 milliseconds and line in time slice 500 milliseconds are the things an interpreter would look for and could be an indication of a geohazard.

[7] See glossary in appendix A.
[8] See glossary in appendix A.

CHAPTER 7

CONCLUSIONS

The aim of this master's thesis is to evaluate whether conventional narrow azimuth streamer 3D data acquired in shallow water can be processed in a new way to sufficiently image the shallow subsurface. To do this has been a problem before and if it can be performed properly a whole new application area opens up for existing data. The answers to two questions of issue could accurately summarise this study; can conventional narrow azimuth 3D data acquired in shallow water be improved for shallow subsurface imaging? If this can be achieved the next question pops up: How may high definition 3D imaging aid dedicated high resolution 2D site survey imaging?

From the investigations the conclusion can be drawn that the new processing sequence do improve the over all imaging of the shallow subsurface for the examined deep target data. This conclusion was drawn when comparing the conventionally processed image to the new processed image for the deep target data. When comparing the high definition processed image to the dedicated high resolution 2D survey image the answer to which one is the best imaging is more nuanced. At the seabed the 2D data clearly gives a better image, than the deep target 3D data high definition image. The high definition 3D processing do still produce reliable information at the seabed horizon [1], which clearly can be seen when comparing 5.25 and 5.26. Comparing (b) and (c) in figure 5.35 gives the understanding that the the dedicated high resolution 2D survey imaging are better resolving the subsurface at near seabed depth. However the high resolution 3D processing increases the image result with depth, relative to the dedicated high resolution 2D survey imaging. How the best imaging changes

[1] See glossary in appendix A.

from the processed 2D data to the high definition processed 3D data can easiest be seen in figure 5.35 to 5.39. To tell an exact depth to where the best imaging is switches cannot be defined exact, but occur somewhere in the range between 200 and 300 milliseconds two-way-time [2].

The fact that the line in 5.42 cannot be distinguished in whole in 5.43, but maybe glimpsed at some parts, indicates the vulnerabilities of a 2D survey. This is why a high definition 3D processed image beforehand the execution of a dedicated high resolution 2D survey can be of good help. Indications of how to set up the 2D survey and how it should be acquired can be of great importance for the ability to image the subsurface and geohazards properly. While the necessity of imaging the first 200 milliseconds properly the dedicated high resolution 2D survey is a must. The aiding in interpretation becomes more notable with depth but as well as 3D effects can be helpful in a shallower stage. Even a less resolved image, as in the first 200 milliseconds two-way-time, can be of great help to indicate such as fault zones. The high definition 3D processing are therefore of great aid in shallow sub seabed imaging and increases with depth, also when data is acquired in shallow water.

To answer the first question: yes, high definition 3D processing can improve convectional narrow azimuth 3D streamer data acquired in shallow water for shallow subsurface imaging, and the improvement increases with depth. The answer to the second question would be: the high definition processed image can aid both prior to the dedicated high resolution 2D survey are conducted as well as in an interpretations stage, especially when an 3D perspective can support the understanding.

[2] See glossary in appendix A.

BIBLIOGRAPHY

Martijn Blaauw, Øyvind Ruden, Annemieke van den Beukel, Kari Berge, and Jostein Haga. Improved geohazards identification, well trajectory selection and drilling performance through high definition seismic. In *Oceanology International*, 2012.

Tim Brice, Michele Buia, Alex Cooke, David Hill, Ed Palmer, Nizar Khaled, Sérgio Tchikanha, Enrico Zamboni, Ed Kotochigov, and Nick Moldoveanu. Developments in full azimuth marine seismic imaging. *Oilfield Review Winter*, 24(4), 2013.

J Bulat. Some considerations on the interpretation of seabed images based on commercial 3d seismic in the faroe-shetland channel. *Basin Research*, 2005.

J Bulat and D Long. Use of 3d seismic data as a substitute for high resolution seismic surveys for site investigation. Reaserch Report 459, British Geological Survey, 2006.

ConocoPhillips. Geophysics, 2015. URL `http://www.conocophillips.com/what-we-do/exploring-for-energy/Pages/geophysics.aspx`.

G. H. F. Gardner, L. W. Gardner, and A. R. Gregory. Formation velocity and density - the diagnostic basics for stratigraphic traps. *Geophysics*, 39(6): 770–780, December 1974.

L. Hatton, M.H. Worthington, and J. Makin. *Seismic Data Processing - theory and practice*. Blackwell Science Ltd, Osney Mead, Oxford OX2 0EL, 1st edition, 1996.

Philip Kearey, Michael Brooks, and Ian Hill. *An introduction to geophysical exploration*. Blackwell Science Ltd, Osney Mead, Oxford OX2 0EL, 3rd edition, 2002.

Gary F. Margrave. Methods of seismic data processing. Published online, 2006. URL http://www.crewes.org/ResearchLinks/FreeSoftware/.

F. Nadim and T.J. Kvalstad. Risk assessment and management for offshore geohazards. In *ISGSR2007 First International Symposium on Geotechnical Safety and Risk*, 2007.

Henry Nainggolan. Seismic forward modelling for syntheric. Published online, 2011. URL http://totalcorner.blogspot.dk/2011/04/seismic-forward-modelling-for-synthetic.html.

Schlumberger. All rights reserved. Oilfield glossary. Published online, 2015. URL http://glossary.oilfield.slb.com/en/.aspx.

J.I. Selvage, C. Jones, C. Scotellaro, Edgar J. A., and Crook H. High resolution interpretation of broad bandwidth 3d seismic data for shallow geohazards. In *74th EAGE Conference Exhibition incorporating SPE EUROPEC*, 2012.

U.S. Geological Survey. Common midpoint method. Published online, 2001. URL http://walrus.wr.usgs.gov/earthquakes/cencal/cmp_methods.html.

Maarten Vanneste. Offshore geohazards, 9 2010. URL http://www.ngi.no/en/Geohazards/Research/Offshore-Geohazards/.

Eric Verschuur. *Seismic multiple removal techniques - past, present and future.* EAGE Publications bv, PO Box 59, 3990 DB HOUTEN, The Netherlands, 1st edition, 2006.

Özdogan Yilmaz. *Seismic data analysis: processing, inversion, and interpretation of seismic data.* Society of Explotation Geophysics, 2nd edition, 2001.

APPENDIX A

GLOSSARY

This appendix will clarify what is intended in this report with expressions often used in the topic of reflection seismology. The expressions described must not be taken as absolute truth but should be close to how most geophysicists use these expression in the geophysical vocabulary.

Clastics — are sedimentary rocks and sediments in transportation.

Common-mid-point (CMP) — the reflecting point for a seismic ray, for this case with flat reflectors the CMP is midway between the source and receiver along the X-axis.

Crossline — "a seismic line within a 3D survey perpendicular to the direction in which the data were acquired" (Schlumberger. All rights reserved., 2015).

Dip — "The magnitude of the inclination of a plane from horizontal. True, or maximum, dip is measured perpendicular to strike. Apparent dip is measured in a direction other than perpendicular to strike." (Schlumberger. All rights reserved., 2015).

Footprints — imaging artifacts due to imperfection compared with an ideal acquisition, for instance appears as lines parallel to the acquisition direction, i.e. inline.

Gather — a gather is a display of traces that share acquisition parameters, such as common-mid-point where the traces share reflection points or common-

source gather where the traces share a source release. To gather is sorting traces that share acquisition parameters performed in processing.

Horizon — a horizontal view of a particular reflection, such as a layer, in a seismic imaged volume. Opposed to horizon is a time slice, from a given time. Horizons "...are convenient displays for visual inspection of seismic attributes..." (Schlumberger. All rights reserved., 2015).

Inline — "a seismic line within a 3D survey parallel to the direction in which the data were acquired. In marine seismic data, the in-line direction is that in which the recording vessel tows the streamers" (Schlumberger. All rights reserved., 2015).

Mute — to subtract selected traces from a stack or gather, which are considered not to contribute accurately to imaging of the subsurface.

Source-receiver offset — "In surface seismic acquisition, the horizontal distance from source to hydrophone" (Schlumberger. All rights reserved., 2015).

Stacking — adding traces in vicinity of a position in the surveyed volume, for the 3D case, or surveyed line, for the 2D case, in processing. These added traces are divided (normalised) somehow to not add up in such as amplitude.

Static correction — often called statics, a shift in time for seismic traces for acquisition circumstances in processing. Statics are performed due to such as water salinity, tide or positioning of the acquisition equipment.

Time slice — "a horizontal display or map view of 3D seismic data having a certain arrival time, as opposed to a horizon slice that shows a particular reflection. A time slice is a quick, convenient way to evaluate changes in amplitude of seismic data" (Schlumberger. All rights reserved., 2015).

Two-way-time (TWT) — the time for the seismic pulse from the source to the receiver via one reflection point, only one reflection. The expression are used if the source and receiver are separated as well as if the position of the source and receiver coincide and the two-way-time is vertical.

APPENDIX B

MATLAB CODE

This is the Matlab code used for producing the synthetic data to investigate the minimum detectable layer. If a subfunction can not be found it is part of the Crewes package.

```
%==========================================
%% Variables
%==========================================

f = f % Dominant frequency in Hz (default: 15 Hz)
dt = dt % Desired temporal sample rate in seconds
dz = dz % Thickness of thin layer
dr = dr % Receiver interval
shotdist = shotdist
firstoff = 100
zlayer = [0;100;200;300-dz/2;300+dz/2;400;500] % Layermodel
velocitymodel = vlayer(1:end-1)
vlayer = vlayer;


%==========================================
%% Define Geometry
%==========================================

% Make strata layer
nlayer = length(zlayer);
```

```
% Input geometry
xmin = 0; xmax = 2100;
zmin = 0; zmax =zlayer(end);
layer = 1:1:nlayer;
thick = abs(diff(zlayer));
dg = 10; xx = xmin:dg:xmax; nx = length(xx);
zz = repmat(zlayer,1,nx);


%================================================
%% Source-Receiver Groups
%================================================

% Source
xs = [xmax/2:-shotdist:0]; % Source positions x-axis
zs = zeros(1,length(xs)); % Source positions z-axis
ns = length(xs);
% Receiver
rec = [0:xmax/2/shotdist]'*-shotdist; %  of receivers
offsetline1=[xmax/2+firstoff:dr:xmax];
recmat = ones(length(rec),1)*offsetline1;
xrall = recmat+rec*ones(1,length(recmat(1,:)));
xr = xrall(1:length(xs),:);
offset = offsetline1-offsetline1(1)+firstoff;
CMP=zeros(size(xr));
for i=1:ns
CMP(i,:) = xs(i)+(xr(i,:)-xs(i))/2; % CMP position created
end
CMPtot = unique(CMP)'; % Unique CMPs
nCMP = length(CMPtot); xrtot = unique(xr);
nxrtot = length(xrtot); zr = zeros(length(xr(1,:)));
nr = length(xr(1,:)); nray = ns*length(unique(xr));


%================================================
%% Create Elastic Parameter
%================================================

% Create synthetic Vp, Vs, and Density
vlayer = vlayer(1:length(zlayer));
vel = [vlayer vlayer];
vp = vlayer; % P wave velocity
vs = (vp-1360)./1.16; % S wave velocity based on Castagna's rule
vs(1) = 0; %No S waves in water
ro = 0.31.*(vp).^0.25;%Density based on Gardner's rule
pois = (vs.^2 - 0.5 * vp.^2)./(vs.^2 - vp.^2);%Poisson ratio
```

```
%PlotGeologyModel
figure; set(gcf,' color',' white');
pcolor(xx, zz, repmat(vlayer, 1, nx)); shadingflat; holdon
colormap(hsv); colorbar('horz');
axis([0xmaxzmin − 0.03 ∗ zmaxzmax])
set(gca,' YDir',' reverse',' XaxisLocation',' bottom', ....
'Ytick', zlayer,' FontWeight',' demi',' PlotBoxAspectRatioMode',' Manual', ...
'PlotBoxAspectRatio', [2.41.21],' Position', [0.040.300.900.60]);


%================================================
%% Run Ray Tracing
%================================================
wat = waitbar(0,'Raytracing is being processed, please wait...');
xoff = [];
% Loop over for number of souce
for i=1:ns
% Plot Source-Receiver Group
plot(xs(i),zs(i),'r*','markersize',12); hold on
plot(xr(i,:),zr,'sk','markersize',4,'markerfacecolor','c'); hold on
xlabel('Velocity (m/s)','FontWeight','bold','Color','black');
ylabel('Depth (m)','FontWeight','bold','Color','black');
% Loop over for number of receiver
for j=1:nr
% Loop over for number of layer
for k=1:nlayer
% Declare reflection boundary
if and(zr(j) ¡ zlayer(k),zs(i) ¡ zlayer(k))
zm = zz(k,:); zf = min(zm)- 100000*eps;
% Downgoing path
d = find(zlayer ¿ zs(i));
if(isempty(d)); sdown = length(zlayer);
else sdown = d(1)-1; end
d = find(zlayer ¿ zf);
if(isempty(d)); edown = length(zlayer);
else edown = d(1)-1; end
zd = [zs(i);zlayer(sdown+1:edown)]; nd = length(zd);
% Upgoing path
u = find(zlayer ¿ zr(j));
if(isempty(u)); sup = length(zlayer);
else sup = u(1)-1; end
u = find(zlayer ¿ zf);
if(isempty(u)); eup = length(zlayer);
else eup = u(1)-1; end
zu = [zr(j);zlayer(sup+1:eup+1)]; nu = length(zu);
zn = [zd;(flipud(zu))]; nrefl = length(zn)-1;
```

```
% Downgoing elastic parameter
vpd = [vp(sdown:edown);vp(edown)];
vsd = [vs(sdown:edown);vs(edown)];
rod = [ro(sdown:edown);ro(edown)];
% Upgoing elastic parameter
vpu = [vp(sup:eup);vp(eup)];
vsu = [vs(sup:eup);vs(eup)];
rou = [ro(sup:eup);ro(eup)];
% Combine model elastic parameter
vpp = [vpd(1:end-1);flipud(vpu(1:end-1))];
vss = [vsd(1:end-1);flipud(vsu(1:end-1))];
vps = [vpd(1:end-1);flipud(vsu(1:end-1))];
rho = [rod(1:end-1);flipud(rou(1:end-1))];
%================================================
% Start Raytracing
theta = abs(teta); twt(k,j,i) = time;
%================================================
% Compute Reflection Coefficient
for y=1:nrefl-1
% Reflection Coefficient of Zoeppritz Approximation
[rc] = zoeppritz(rho(y),vpp,vss(y),rho(y+1),vpp(y+1),vss(y+1),1,1,1,theta(y)
dir = imag(rc)/abs(imag(rc)); rcz(y,j,i) = real(dir*rc);
end
%================================================
end
end % for horizon/reflector end
xoff = [xoff xr(i,j)]; waitbar(j/nray,wat)
end % for receiver end
waitbar(i/ns,wat)
end % for sources end
close(wat); xrtot = unique(xr)';
xx = repmat(offset,nlayer,1);
tt=twt; % Travel times
reflz=rcz; % Reflection coefficient results


%================================================
%% AVO Modelling
%================================================
% Make Ricker wavelet
dt = dt; f = f;
[w,tw] = ricker(dt,f);
% Create zeros matrix for spike's location
tmax = max(tt(:));
tr = 0:dt:tmax; nt = length(tr);
t = tt(2:nlayer,:,:);
```

```
% Take reflectivity into spike's location
spikes = zeros(nt,nr,ns); rczz = real(reflz(1:nlayer-1,:,:));
for i=1:ns
for k=1:nlayer-1
for j=1:nr
ir(k,j,i) = round(t(k,j,i)/dt+0.0)+0;
spikes(ir(k,j),j,i) = spikes(ir(k,j),j,i) + rczz(k,j,i);
end
end
end
% Convolve spikes with Ricker wavelet
seisz = [];
for i=1:ns
for j=1:nr
seisz(:,j,i) = convz(spikes(:,j,i),w);
end
end
ampz = seisz;
ampzfirst = zeros(size(ampz));
ampzfirst(:,1,:) = ampz(:,1,:);


%================================================
%% NMO Modelling
%================================================
[nz,nx,ni] = size(ampz);
avevel = cumsum(2*thick)./cumsum((2*thick)./vlayer(1:end-1));
velocitymodel = avevel
cumthick=cumsum(thick);
ampz2 = [];
for i = 1:ns
ampz2(:,:,i) = [ampz(:,:,i); zeros(10,nx)];
end
datatest = zeros(size(ampz(:,:,1)));
outdata = zeros(size(ampz));
% NMO correction sequence
for k = 1:ns
for i = 1:length(thick)-1
t0m = (cumthick(i)/avevel(i))*2;
tstop = sqrt((t0m)^2 + offset.^2./avevel(i)^2);
nstop = round(tstop/dt);
nm = round(t0m/dt);
forh = 1 : numel(nstop)
datatest(nstop(h), h, k) = 10;
tempdata = ampz2(nstop(h) - 25 : nstop(h) + 25, h, k);
forj = -25 : 25
```

$if outdata(nm + j, h, k) == 0$
$outdata(nm + j, h, k) = tempdata(j + 26);$
end
end
end
end
end

```
%================================================
%% Mute NMO Corrected Data
%================================================
mutedata = outdata;
if iter == 1
mute = input('Is mute necessary? 1 for YES, 0 for NO ');
if mute  = 1  mute  = 0
mute = input('Second try: Is mute necessary? 1 for YES, 0 for NO ');
end
if mute  = 0
d1 = input('Start of mute ') ;
d1step = input('Mute angle clockwise from horizontal, degrees ');
end
elseif iter == 2
change = input('Do you want to change mute? Second chance, out of 3. 1 for
YES, 0 for NO ');
if change  = 1  change  = 0
mute = input('Second try: Do you want to change mute? Last chance this
round. 1 for YES, 0 for NO ');
end
if change  = 0
mute = input('Is mute necassary? 1 for YES, 0 for NO ');
if mute  = 1  mute  = 0
mute = input('Secon d try: Is mute necessary? 1 for YES, 0 for NO ');
end
if mute  = 0
d1 = input('Start of mute ') ;
d1step = input('Mute angle clockwise from horizontal, degrees ');
end
end
elseif iter == 3
change = input('Do you want to change mute? Last chance. 1 for YES, 0 for
NO ');
if change  = 1  change  = 0
mute = input('Second try: Do you want to change mute? Last chance this
round. 1 for YES, 0 for NO ');
end
```

```
if change  = 0
mute = input('Is mute necassary? 1 for YES, 0 for NO ');
if mute  = 1  mute  = 0
mute = input('Secon d try: Is mute necessary? 1 for YES, 0 for NO ');
end
if mute  = 0
d1 = input('Start of mute ') ;
d1step = input('Mute angle clockwise from horizontal, degrees ');
end
end
end
if mute  = 0
ratio = tand(d1step);
step = round(ratio*numel(tr)/numel(CMP(1,:)));
for i = 1:ns
for j = d1:nx
d11 = (j-d1+1)*step;
if d11 ¿ nz
d11 = nz;
mutedata(1:d11,j,i) = 0;
else
mutedata(1:d11,j,i) = 0;
end
end
end
end
% Sorting NMO Corrected  Muted Data
sortdata = zeros(nt,nCMP,ns);
for i = 1:ns
xstart = sum(CMP(i,1)¿=CMPtot);
sortdata(:,xstart:xstart+nx-1,i) = mutedata(:,:,i);
end
% CMP Stacked
Stacked = zeros(size(sortdata(:,:,1)));
divmat = ones(size(sortdata(:,:,1)));
for i=1:ns
divmat = divmat + (sortdata(:,:,i) =0);
Stacked = Stacked + sortdata(:,:,i);
end
Stacked = Stacked./divmat; % Stacked and Normalized


%================================================
%% % Plot
%================================================
figure
```

```
wig(CMPtot,tr,Stacked,'black'); hold on
xlabel('CMP (m)','FontWeight','bold','Color','black');
ylabel('Time (s)','FontWeight','bold','Color','black');
title('Synthetic Seismogram, Stacked','FontWeight','bold','Color','black');
axis tight
set(gca,'YColor',[0.04314 0.5176 0.7804],'XColor',[0.04314 0.5176 0.7804]); hold
on
set(gcf,'color','white');
```

APPENDIX C

EXTRA SYNTHETIC RESULTS

Additional results from the synthetic modelling are presented in this appendix C in the web published version. The extra results are presented without the red arrow indicating the target layer. For an indication of the target layer and explanation of the displays please see section 5.1. Every figure displays three subfigures, each subfigure is one result. Only results not presented in section 5.1 are presented in this appendix C. The reader is recommended to examine the results below on a computer screen with the ability to zoom in.

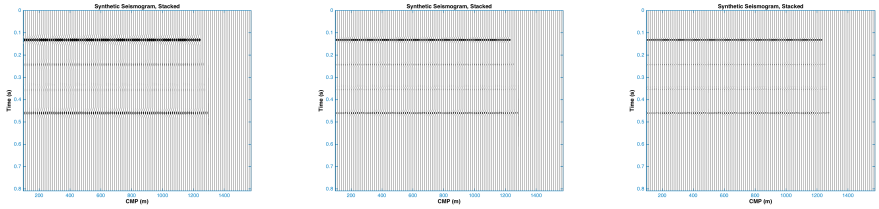

(a) (b) (c)

Figure C.1: (a)Target layer: 2 m, 1600 m/s. Dominant frequency of source wavelet 30 Hz. (b)Target layer: 2 m, 1600 m/s. Dominant frequency of source wavelet 50 Hz. (c)Target layer: 2 m, 1600 m/s. Dominant frequency of source wavelet 70 Hz.

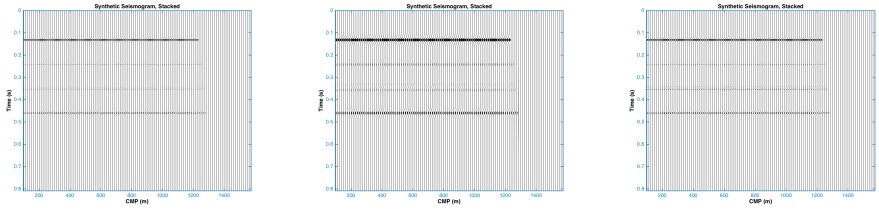

(a) (b) (c)

Figure C.2: (a)Target layer: 2 m, 1600 m/s. Dominant frequency of source wavelet 90 Hz. (b)Target layer: 4 m, 1600 m/s. Dominant frequency of source wavelet 30 Hz. (c)Target layer: 4 m, 1600 m/s. Dominant frequency of source wavelet 70 Hz.

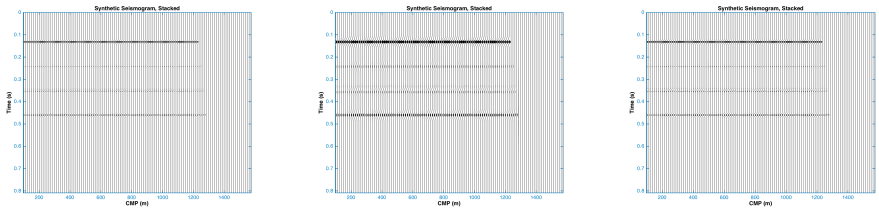

(a) (b) (c)

Figure C.3: (a)Target layer: 4 m, 1600 m/s. Dominant frequency of source wavelet 90 Hz. (b)Target layer: 6 m, 1600 m/s. Dominant frequency of source wavelet 30 Hz. (c)Target layer: 6 m, 1600 m/s. Dominant frequency of source wavelet 70 Hz.

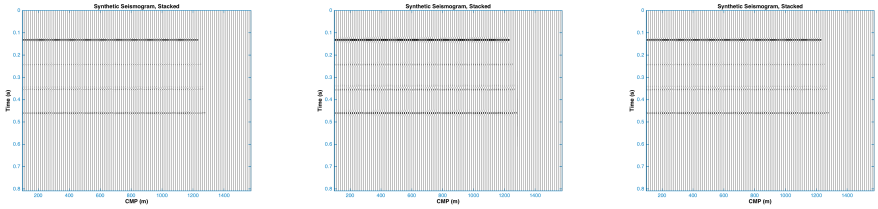

(a) (b) (c)

Figure C.4: (a)Target layer: 6 m, 1600 m/s. Dominant frequency of source wavelet 90 Hz. (b)Target layer: 8 m, 1600 m/s. Dominant frequency of source wavelet 50 Hz. (c)Target layer: 8 m, 1600 m/s. Dominant frequency of source wavelet 70 Hz.

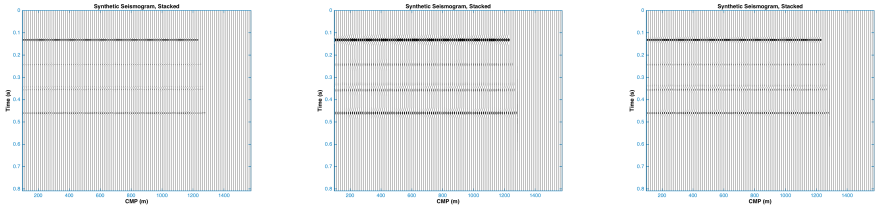

(a) (b) (c)

Figure C.5: (a)Target layer: 8 m, 1600 m/s. Dominant frequency of source wavelet 90 Hz. (b)Target layer: 10 m, 1600 m/s. Dominant frequency of source wavelet 30 Hz. (c)Target layer: 10 m, 1600 m/s. Dominant frequency of source wavelet 50 Hz.

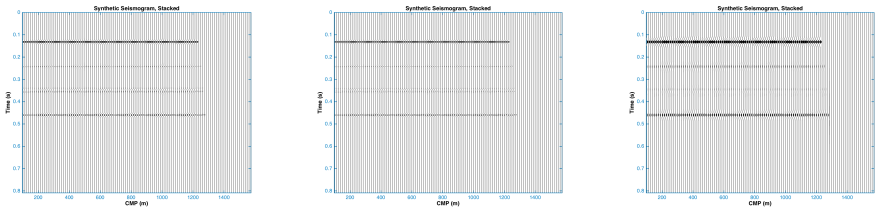

(a) (b) (c)

Figure C.6: (a)Target layer: 10 m, 1600 m/s. Dominant frequency of source wavelet 70 Hz. (b)Target layer: 10 m, 1600 m/s. Dominant frequency of source wavelet 90 Hz. (c)Target layer: 2 m, 1800 m/s. Dominant frequency of source wavelet 30 Hz.

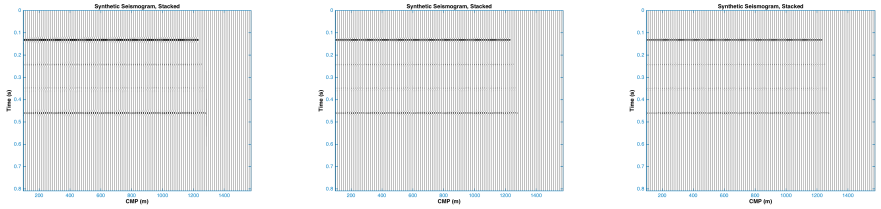

(a) (b) (c)

Figure C.7: (a)Target layer: 2 m, 1800 m/s. Dominant frequency of source wavelet 50 Hz. (b)Target layer: 2 m, 1800 m/s. Dominant frequency of source wavelet 70 Hz. (c)Target layer: 2 m, 1800 m/s. Dominant frequency of source wavelet 90 Hz.

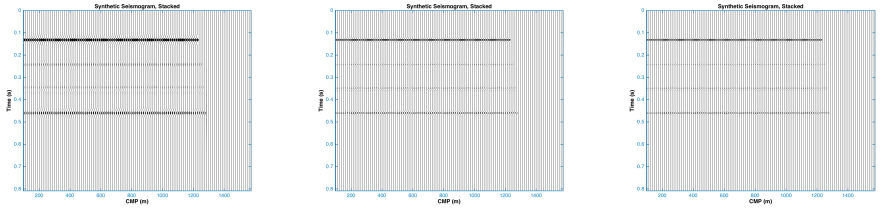

(a) (b) (c)

Figure C.8: (a)Target layer: 4 m, 1800 m/s. Dominant frequency of source wavelet 30 Hz. (b)Target layer: 4 m, 1800 m/s. Dominant frequency of source wavelet 70 Hz. (c)Target layer: 4 m, 1800 m/s. Dominant frequency of source wavelet 90 Hz.

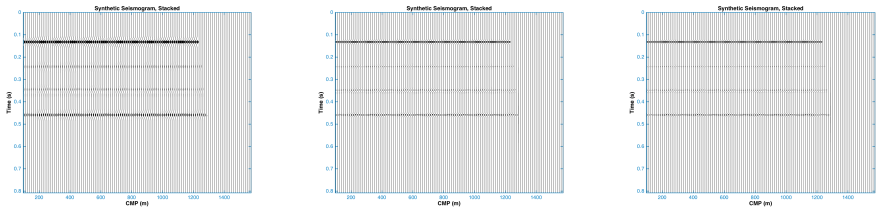

(a) (b) (c)

Figure C.9: (a)Target layer: 6 m, 1800 m/s. Dominant frequency of source wavelet 30 Hz. (b)Target layer: 6 m, 1800 m/s. Dominant frequency of source wavelet 70 Hz. (c)Target layer: 6 m, 1800 m/s. Dominant frequency of source wavelet 90 Hz.

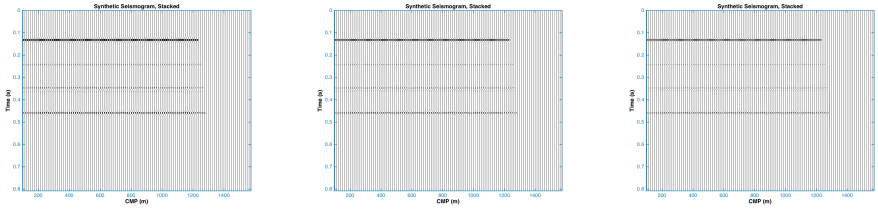

(a) (b) (c)

Figure C.10: (a)Target layer: 8 m, 1800 m/s. Dominant frequency of source wavelet 50 Hz. (b)Target layer: 8 m, 1800 m/s. Dominant frequency of source wavelet 70 Hz. (c)Target layer: 8 m, 1800 m/s. Dominant frequency of source wavelet 90 Hz.

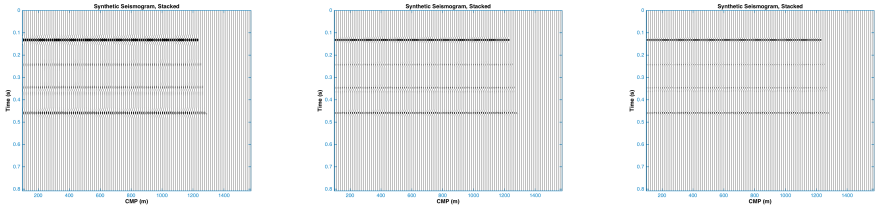

(a) (b) (c)

Figure C.11: (a)Target layer: 10 m, 1800 m/s. Dominant frequency of source wavelet 30 Hz. (b)Target layer: 10 m, 1800 m/s. Dominant frequency of source wavelet 50 Hz. (c)Target layer: 10 m, 1800 m/s. Dominant frequency of source wavelet 70 Hz.

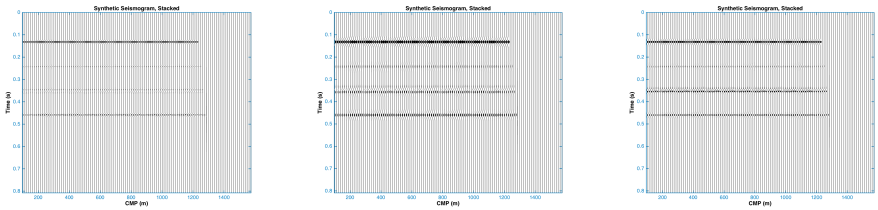

(a) (b) (c)

Figure C.12: (a)Target layer: 10 m, 1800 m/s. Dominant frequency of source wavelet 90 Hz. (b)Target layer: 2 m, 1900 m/s. Dominant frequency of source wavelet 30 Hz. (c)Target layer: 2 m, 1900 m/s. Dominant frequency of source wavelet 50 Hz.

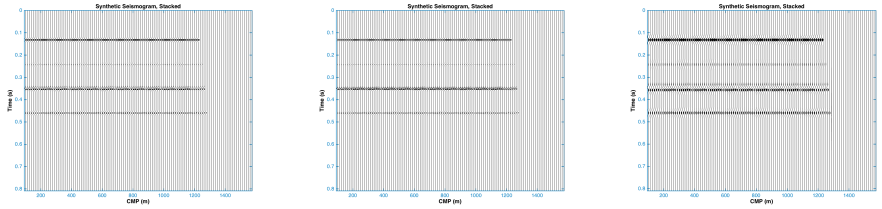

(a) (b) (c)

Figure C.13: (a)Target layer: 2 m, 1900 m/s. Dominant frequency of source wavelet 70 Hz. (b)Target layer: 2 m, 1900 m/s. Dominant frequency of source wavelet 90 Hz. (c)Target layer: 4 m, 1900 m/s. Dominant frequency of source wavelet 30 Hz.

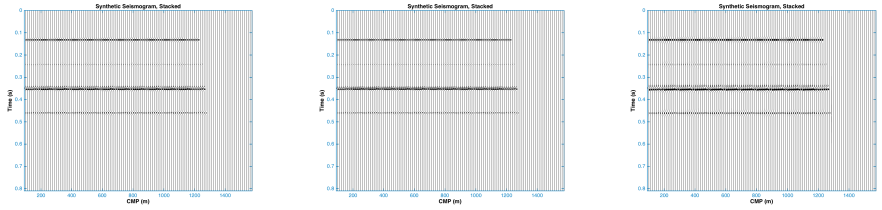

(a) (b) (c)

Figure C.14: (a)Target layer: 4 m, 1900 m/s. Dominant frequency of source wavelet 70 Hz. (b)Target layer: 4 m, 1900 m/s. Dominant frequency of source wavelet 90 Hz. (c)Target layer: 6 m, 1900 m/s. Dominant frequency of source wavelet 50 Hz.

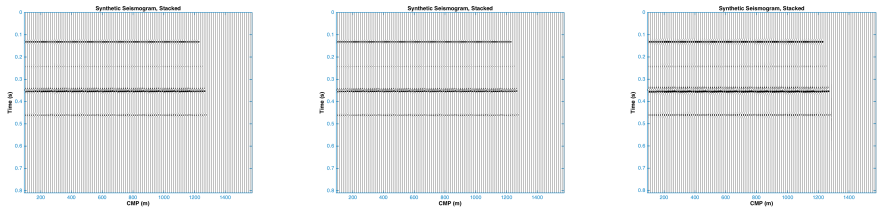

(a) (b) (c)

Figure C.15: (a)Target layer: 6 m, 1900 m/s. Dominant frequency of source wavelet 70 Hz. (b)Target layer: 6 m, 1900 m/s. Dominant frequency of source wavelet 90 Hz. (c)Target layer: 8 m, 1900 m/s. Dominant frequency of source wavelet 50 Hz.

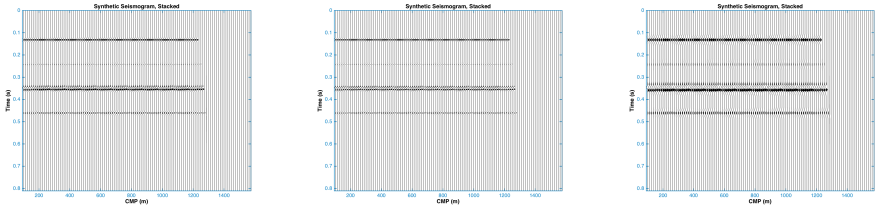

(a) (b) (c)

Figure C.16: (a)Target layer: 8 m, 1900 m/s. Dominant frequency of source wavelet 70 Hz. (b)Target layer: 8 m, 1900 m/s. Dominant frequency of source wavelet 90 Hz. (c)Target layer: 10 m, 1900 m/s. Dominant frequency of source wavelet 30 Hz.

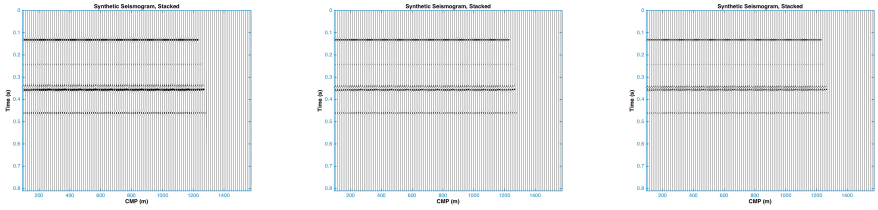

(a) (b) (c)

Figure C.17: (a)Target layer: 10 m, 1900 m/s. Dominant frequency of source wavelet 50 Hz. (b)Target layer: 10 m, 1900 m/s. Dominant frequency of source wavelet 70 Hz. (c)Target layer: 10 m, 1900 m/s. Dominant frequency of source wavelet 90 Hz.

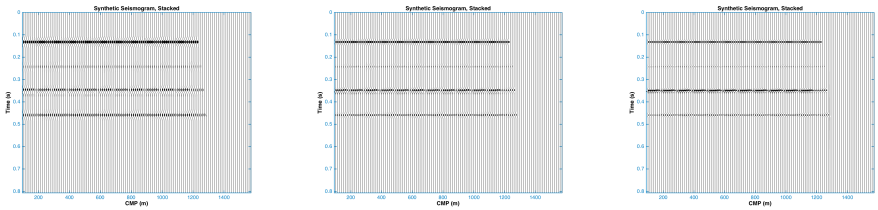

(a) (b) (c)

Figure C.18: (a)Target layer: 2 m, 2500 m/s. Dominant frequency of source wavelet 30 Hz. (b)Target layer: 2 m, 2500 m/s. Dominant frequency of source wavelet 50 Hz. (c)Target layer: 2 m, 2500 m/s. Dominant frequency of source wavelet 70 Hz.

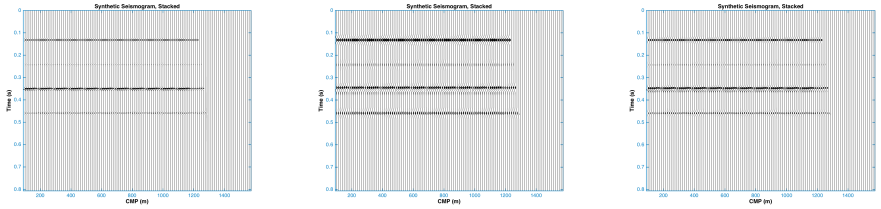

(a) (b) (c)

Figure C.19: (a)Target layer: 2 m, 2500 m/s. Dominant frequency of source wavelet 90 Hz. (b)Target layer: 4 m, 2500 m/s. Dominant frequency of source wavelet 30 Hz. (c)Target layer: 4 m, 2500 m/s. Dominant frequency of source wavelet 50 Hz.

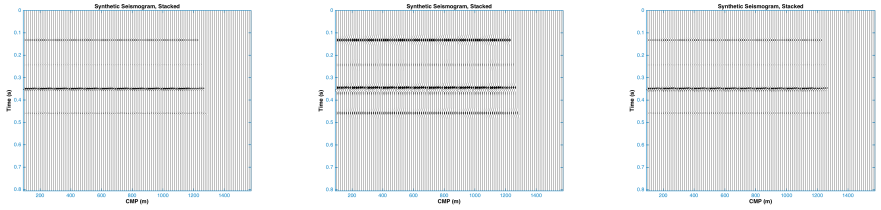

(a) (b) (c)

Figure C.20: (a)Target layer: 4 m, 2500 m/s. Dominant frequency of source wavelet 90 Hz. (b)Target layer: 6 m, 2500 m/s. Dominant frequency of source wavelet 30 Hz. (c)Target layer: 6 m, 2500 m/s. Dominant frequency of source wavelet 70 Hz.

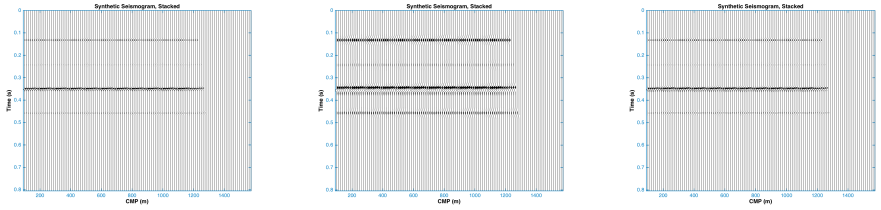

(a) (b) (c)

Figure C.21: (a)Target layer: 6 m, 2500 m/s. Dominant frequency of source wavelet 90 Hz. (b)Target layer: 8 m, 2500 m/s. Dominant frequency of source wavelet 30 Hz. (c)Target layer: 8 m, 2500 m/s. Dominant frequency of source wavelet 70 Hz.

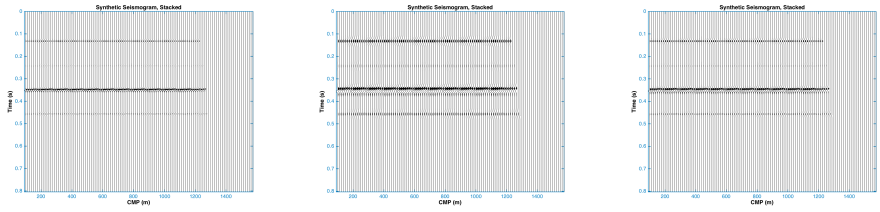

(a) (b) (c)

Figure C.22: (a)Target layer: 8 m, 2500 m/s. Dominant frequency of source wavelet 90 Hz. (b)Target layer: 10 m, 2500 m/s. Dominant frequency of source wavelet 30 Hz. (c)Target layer: 10 m, 2500 m/s. Dominant frequency of source wavelet 50 Hz.

(a) (b)

Figure C.23: (a)Target layer: 10 m, 2500 m/s. Dominant frequency of source wavelet 70 Hz. (b)Target layer: 10 m, 2500 m/s. Dominant frequency of source wavelet 90 Hz.